JAN.- APR. 2005
Volume XI Number I
ISSN 0859 144X

THE ASEAN JOURNAL OF RADIOLOGY

Published by The Radiological Society and
The Royal College of Radiologists of Thailand,
Bangkok, Thailand

Started through an educational grant from Bracco since 1995

JAN. - APR. 2005
Volume XI Number I

ISSN 0859 144X

THE ASEAN JOURNAL OF RADIOLOGY

**Published by The Radiological Society and
The Royal College of Radiologists of Thailand,
Bangkok, Thailand**

Started through an educational grant from Bracco since 1995

Chief Editor

Professor Kawee Tungsubutra
Kaweevej Hospital, 318 Taksin Road, Dhonburi, Bangkok 10600, Thailand.

Asean Journal of Radiology.
Instructions for Authors.

1. The Asean Journal of Radiology publishes the papers on Radiological Sciences, such as research work, review articles, case reports, innovations in Medical Sciences related to all branches of Radiology, and letters to the editor. The aforementioned materials can be written in English only.

2. The authors have to submit 2 copies of the manuscript and a diskette: **to Prof. Dr. Kawee Tungsubutra.** 318 Kaweevej Hospital, Taksin Road, Dhonburi, Bangkok 10600, Thailand.

3. The original copy to be submitted must be typed in a double space on one side of the page of 8.1/2" x 11.1/2" paper.

4. The format of the article must include :
   a. Title page and address of the author (s)
   b. Abstract
   c. Introduction (Background)
   d. Material and Method
   e. Results and discussion (Tables and Illustrations)
   f. Acknowledgement (if any)
   g. References (Follow the Vancouver style developed by ICMJE)

5. We will provide 5 copies of reprints for the author (s) who submit (s) an article for publication in the Asean Journal.

6. The illustrations and tables must be clearly prepared with legends in English as they are the art works to be reproduced.

7. The authors are reponsible for the contents of the article as to its facts and findings.

8. Ethics.

Paper reporting studies which might be interpreted as human experimentation (e.g. controlled trials) should conform to the standards of the Declaration of Helsinki (see British Medical Journal 1964: 2: 177) and should indicate that, approval that such studies may proceed, has been granted by the local or hospital Ethics Committee.

When reporting experiments on animals indicate whether the institution's or the National Research Council's guide for, or any national law on, the care and use of laboratory animals was followed.

THE ASEAN JOURNAL OF RADIOLOGY

Volume XI Number I JAN.-APR. 2005

CONTENTS

THE ASEAN JOURNAL OF RADIOLOGY

Volume XI Number I JAN.-APR. 2005

CONTENTS

CURRENT TOPICS IN IMAGING OF JUVENILE RHEUMATOID ARTHRITIS

Preeyacha PACHARN, M.D.[1], Kullanuch CHANCHAIRUJIRA, M.D.[1]
Thomas J.BRYCE, M.D.[2], Thaschawee ARKACHAISRI, M.D.[3]

INTRODUCTION

Juvenile rheumatoid arthritis (JRA) is diagnosed when arthritis is identified in a child aged 16 or younger, lasting 6 weeks or more, in whom other causes of childhood arthritis are excluded. The disease is more commonly found in Caucasian children than African or Asian children.[1] JRA typically demonstrates more rapid progression of disease compared with adult rheumatoid arthritis and can significantly impair bony development in the growing child.

According to the American College of Rheumatology, JRA can be classified into three categories based on number and joints involved, symptoms and the presence of specific antibodies.

(1) The pauciarticular form is the most common form of JRA, involving 4 or less joints.
(2) The poly articular form, in which 5 or more joints are involved.
(3) The systemic form of JRA, or "Still's disease." In this subtype, other organs are sometimes involved. The patients usually develop high fever with rash.

The symptoms of JRA include swollen, stiff, erythematous and painful joints. High fever with rash, lymphadenopathy and fatigue can be seen in systemic JRA. Early diagnosis is crucial. However, there is no single 'gold standard' diagnostic test for JRA. Diagnosis is based on a variety of data including clinical signs and symptoms. There are a large variety of synovial and non-synovial conditions which may mimic JRA[2] Therefore, a careful history and physical examination combined with imaging studies should help to distinguish these conditions from JRA, especially in cases with an unusual clinical presentation. During treatment, imaging plays a key role in the evaluation of disease progression and in monitoring the effect of therapy.

Plain radiography

Plain radiographs have traditionally been the primary imaging modality used to aid the diagnosis. They are the most cost-effective examination in the exclusion of the alternated diagnoses.[3] Early in the disease course, plain radiographs sometime show soft tissue swelling, joint effusions, periosteal new bone formation or accelerated maturation of the epiphysis.[2,4] (fig.1) Soft tissue swelling is usually seen after the first week, resulting from periarticular edema, synovial proliferation and accumulation of joint fluid.[5] However, these findings are nonspecific and may be seen in a variety of inflammatory arthritides.

[1] Departments of Radiology Siriraj Hospital, Mahidol University
[2] Department of Radiology, University of California San Francisco
[3] Pediatrics Siriraj Hospital, Mahidol University

Some findings appear late in the course of disease when substantial bone and joint damage has occurred. Periarticular osteopenia can be seen on plain radiographs when there is at least 30% -50% loss of bone mineralization.[6] Joint space narrowing is indirect evidence of articular cartilage damage and bone erosions are seen after significant cartilage loss has occured. These late changes are usually irreversible. (fig.2)

The lack of specificity of radiographs has resulted in an increase in the use of ultrasound and MRI, which are more sensitive in detecting intra -articular abnormalities.

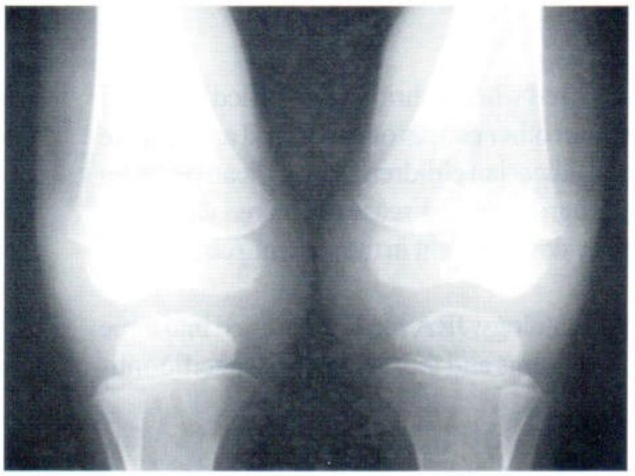

Fig.1A

Fig.1B

Fig.1B

Fig.1 4-year-old girl with history of JRA. Plain radiographs were obtained at the early diagnosis. Plain radiograph of the both knees, AP (A) and lateral (B) view demonstrated marked soft tissue swelling and mild enlargement of epiphysis.

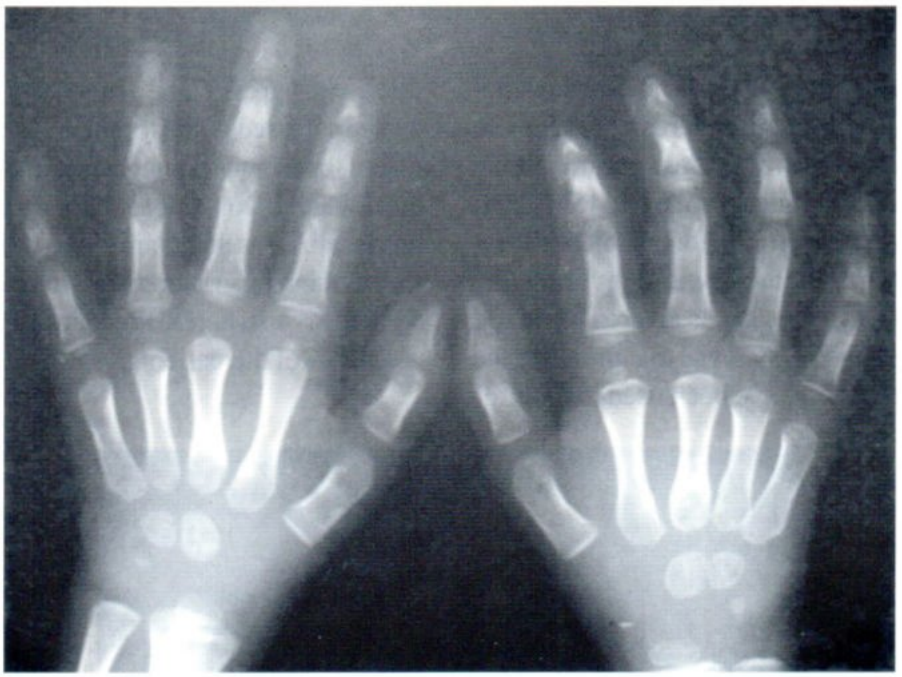

Fig.1 4-year-old girl with history of JRA. Plain radiographs were obtained at the early diagnosis. (C), Plain radiograph of both hands showed soft tissue swelling with no definite bony destruction.

Fig.2 8-year-old girl with JRA Plain radiograph showed diffuse narrowing of carpometacarpal, intercarpals and radiocarpal joint spaces of both hands. There are some erosions of carpal bones.

Ultrasonography

Ultrasound is more sensitive than plain radiographs in detecting cartilaginous erosions, synovial thickening and effusions, but is less sensitive than MRI.[3] A high frequency linear probe (12-15MHz) is usually used. A simple joint effusion is almost always anechoic.(fig.3) An inflamed synovium lining the articular cartilage can be seen as an area of mixed echogenicity.(fig.4A) The Synovial thickness and the amount of joint effusion have been used to monitor disease progress.[7] The vascularity of the synovium can be assessed with Doppler examination. Hyperemia of the pannus is suggestive of the active phase of the disease. Involvement of the articular cartilage can be visualized as thickening in early stages (fig.4B) as well as thinning in later stages. Blurring of the articular cartilage is also noted. Popliteal cysts may be seen in upto 40% of the patients.[5]

Fig.3A

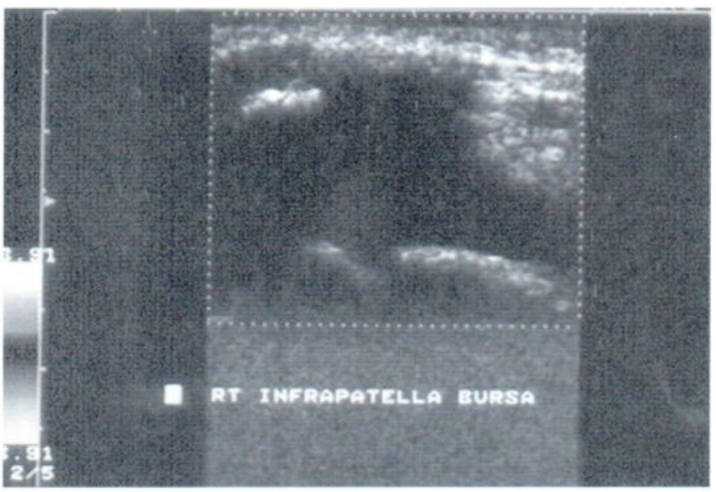

Fig.3B

Fig.3 5-year-old boy with JRA Ultrasound of the right knee at the level of suprapatella bursa (A) and infrapatella bursa (B) demonstrated fluid echogenicity of simple joint effusion.

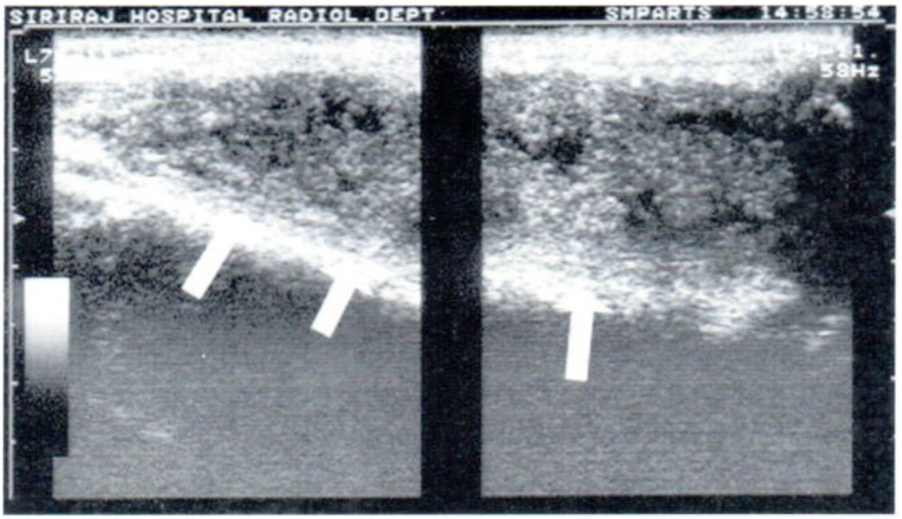

Fig.4A

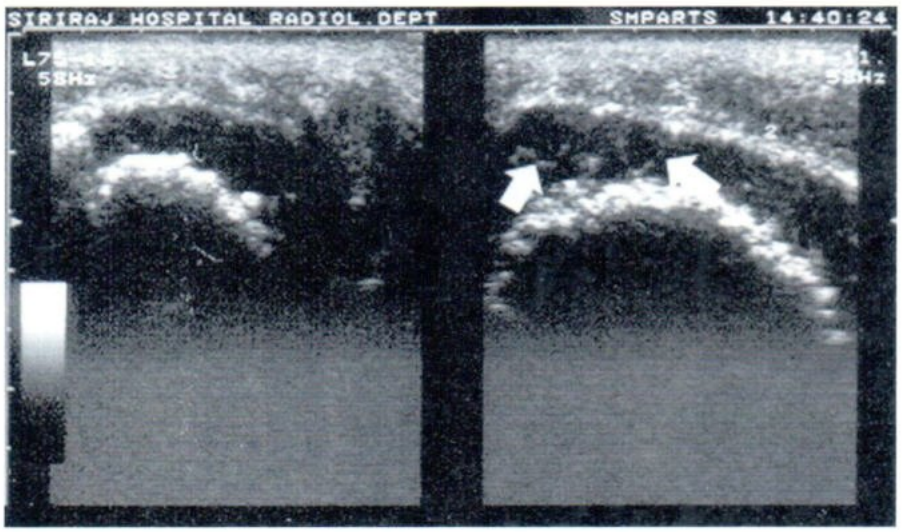

Fig.4B

Fig.4 5-year-old boy with JRA and swelling of both knees (A),Ultrasound of the right knee at the right suprapatella bursa showed distend right suprapatella bursa with mixed echogenic material and thickening of synovial lining.(arrows) (B), Involvement of the articular cartilage in the early stage showed thickening of the cartilage. Hyperechoic strands (arrows) are related to hyperemic vessels.

The advantages of ultrasound are relatively short examination time, noninvasiveness, ease of side to side comparison. However, the technique is operator dependent and requires patient cooperation. It may be difficult to perform in small children. Ultrasound can also be used to aid the aspiration or therapeutic injection of affected joints.

Magnetic resonance imaging (MRI)

MRI is the most sensitive radiologic indicator of disease activity. Because of its excellent soft tissue contrast, synovial hypertrophy, articular cartilage and joint effusions can be clearly demonstrated.[2,8] Peripheral soft tissue can be visualized.

Many pulse sequences are available and different sequences are appropriate for different structures. The selection of examination protocols should be based on the pertinent clinical questions. A small field of view should be used with thin slice thickness.

Bony erosions can be seen using regular T1W and T2W sequences. Hypertrophic synovium is best demonstrated on post Gd-DTPA T1W images with fat suppression. Fibrous, nonvascular synovium is seen as low signal intensity (SI) on both T1W and T2W sequences with no Gd-DTPA enhancement, while inflamed hypervascular synovium shows low SI on T1W sequences and high SI on T2W sequences or T1W sequences with Gd-DTPA enhancement. In inflamed joints, marked enhancement of the thickened nodular or villous synovium is usually identified.[9,10] (fig.5,6) A maximal synovial thickness of 3 mm or more yielded 100% specificity and 77% sensitivity for the diagnosis of synovitis.[10]

Even though synovial enhancement is a non-specific finding, the clinical history and physical examination will be helpful in the exclusion of infection or other joint diseases.

Fig.5A

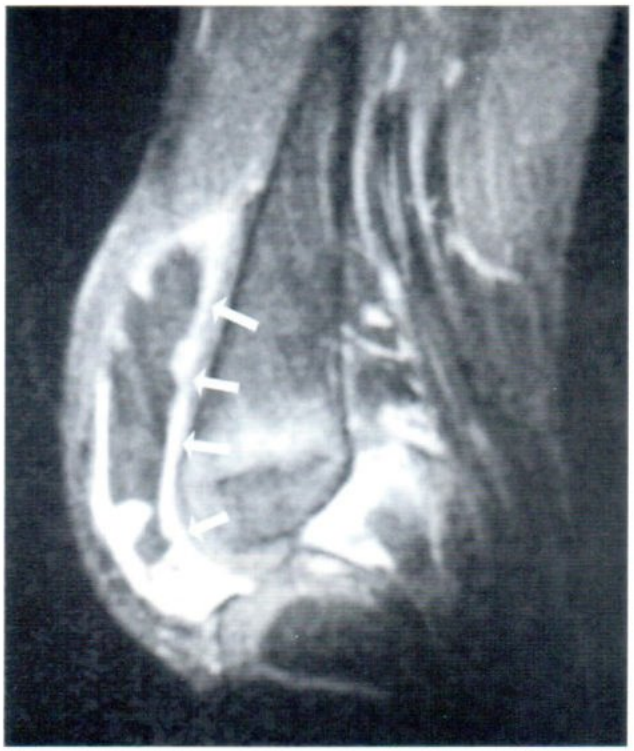

Fig.5B

Fig.5 5-year-old boy with JRA
(A), Sagittal T1weighted image of the right knee showed distension of prepatella bursa with intermediate signal intensity mass like structure, cannot differentiated between thickening synovium and joint fluid. Sagittal T1 weighted after Gd-DTPA enhancement (B) markedly enhancement of thicken synovial tissue is demonstrated. (arrows)

Fig.5C

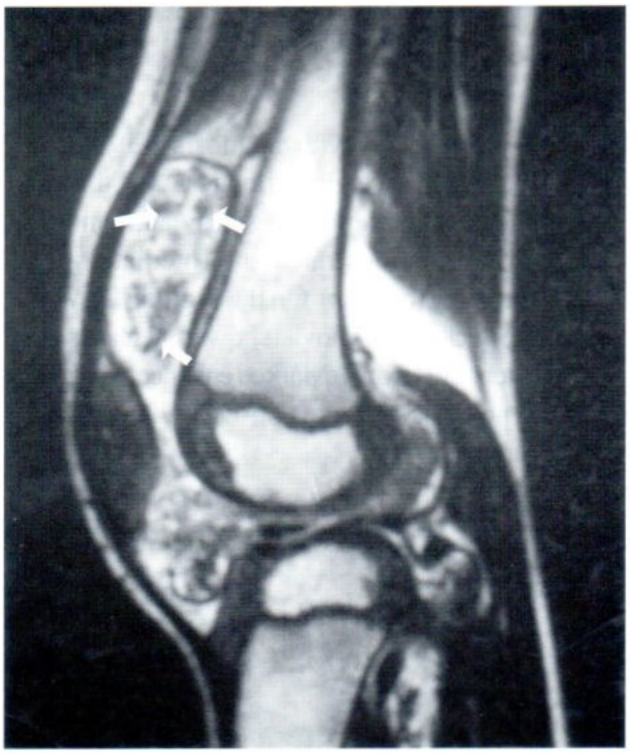

Fig.5D

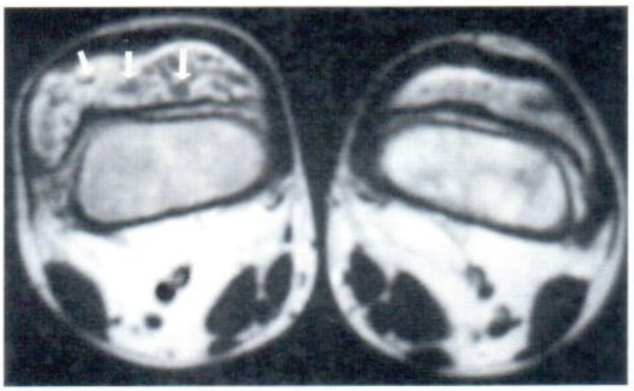

Fig.5E

Fig.5 5-year-old boy with JRA
(C), Coronal T1weight with fat suppression technique and Gd-DTPA enhancement showed vivid enhancement of inflammed synovium in the active phase of disease.(arrows) Sagittal (D) and axial (E) T2weighted images showed synovial membrane with relatively high signal intensity with some joint fluid. Multiple hypo-signal intensity structures, resembling grains of rice inside the joint space is the slough off synovial villi, so called "rice body."(arrows)

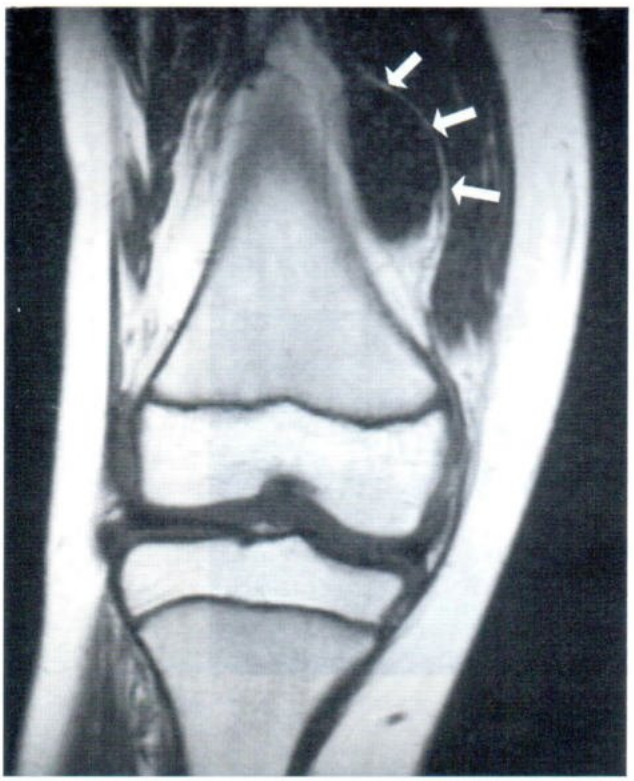

Fig.6A

Fig.6B

Fig.6C

Fig.6 8-year-old boy with diagnosis of JRA Coronal T1weighted image (A) of the knee showed thickening of synovial membrane which demonstrated intermediate signal intensity.(arrows) On the sagittal T2W (B), the thickening synovial showed increase signal intensity.(arrows) Marked enhancement of the synovial is seen after Gd-DTPA injection.(C) (arrows)

Joint effusions show fluid signal intensity, low on T1W and high on T2W sequences(fig.7), which is easily differentiated from inflammed synovium on post Gd-DTPA T1W images.

Articular cartilage is also important because it is one of the earliest structures to demonstrate disease involvement and damage. Cartilage is best demonstrated on FSE T2W or FSE proton density sequences with fat suppression. Cartilage demonstrates high signal intensity on these two sequences. Areas of altered signal intensity, thinning and erosions should be looked for.

A major limitation of MRI is relatively long examination time. The majority of children up to 4-5 years of age require sedation.[11] MRI is also the most costly of the primary imaging modalities for JRA.

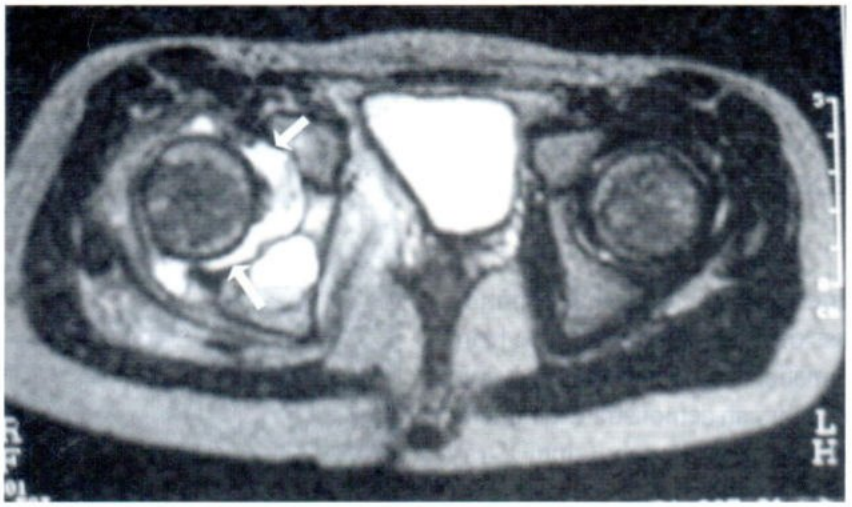

Fig.7A

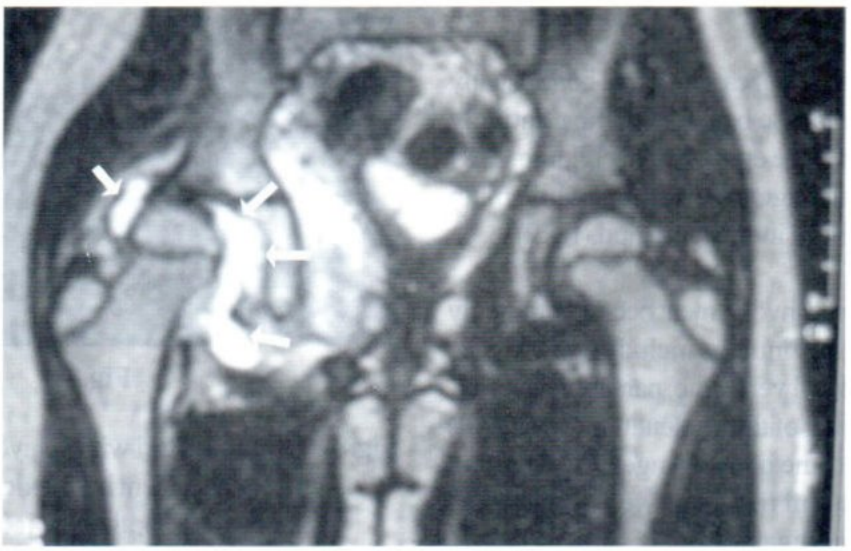

Fig.7B

Fig.7 6-year-old girl with chronic hip pain and diagnosis of JRA Axial (A) and coronal (B) T2weighted images of both hips shows high signal intensity, indicating right hip joint effusion. (arrows)

Complications

Chronic inflammation in JRA results in growth disturbance which can manifest after a few months. (fig.8) Growth disturbance results from hyperemia of the affected joints. Accelerated maturation of the epiphyseal ossification centers, round bones, and sessamoids, and a bulbous appearance of the proximal phalanges can be seen. If the disease occurs before physeal fusion, limb shortening is more likely.[3]

Early treatment will limit growth disturbance. Therefore, there has been an increase in the use of ultrasound and MRI, which are more accurate in the detection of active disease compared with traditional plain radiographs.

Bony demineralization is another common feature of JRA. Loss of bone density may be from hypervascular inflammation, immobilization, or steroid therapy. Plain radiographs can demonstrate demineralization when bone loss is marked, but dual X-ray absorptiometry is more sensitive for lesser degrees of demineralization and is more accurate in monitoring bone mineralization changes.

Erosive changes of cartilage and bone usually appear late in the disease because of the relatively thick cartilage around the epiphyses in children. MRI can detect early cartilage involvement while plain radiographs are only an indirect method.(fig.9)

Cervical spine involvement occurs commonly in polyarticular JRA. Findings include bony fusion, remodelling of cervical vertebrae, paraspinous calcification, and widening of the predental space.(fig.10) Plain film can detect the bony changes, but MRI can be used to evaluate soft tissues as well as the spinal cord and paraspinous ligaments.

Fig.8A

Fig.8B

Fig.8 8-year-old girl with delayed diagnosis of JRA (A), The patient has flexion deformity of both elbows and both knee joints.
(B), Close up image shows marked soft tissue swelling of both hands with fusiform shape of the digits.

Fig.8C

Fig.8 8-year-old girl with delayed diagnosis of JRA (C), Fusion of her left elbow joint is demonstrated.

Fig.9 15-year-old with chronic JRA
Plain radiograph of both hips demonstrated narrowing of both hips joint spaces which reflected the destruction of articular cartilages.

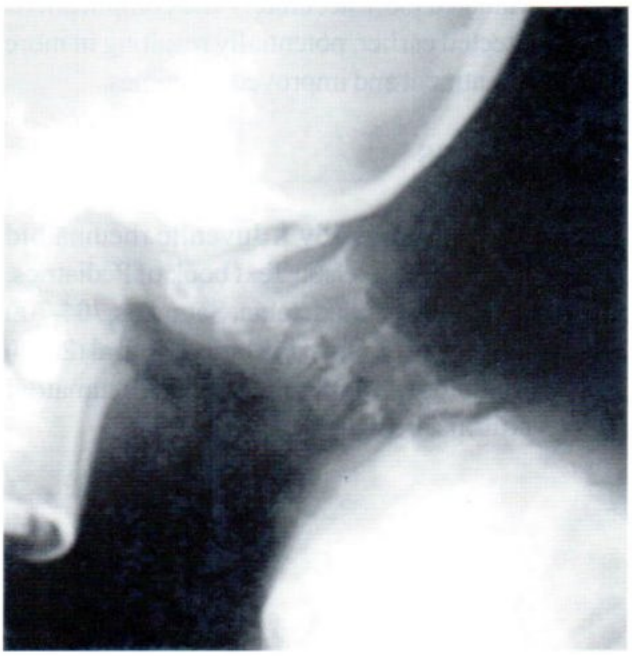

Fig.10 Fusion of cervical spine in a chronic JRA patient.

CONCLUSIONS

JRA is a serious condition which can result in growth disturbance and disability in children. Several imaging modalities are employed for diagnosis and follow up.

Plain film is still quite useful and cost-effective. It may be an appropriate first radiological exam, particularly to exclude alternate diagnoses. However, in children with an atypical presentation, ultrasound or MRI should be considered given that more information about intraarticular structures and processes are provided by these exams, potentially allowing greater specificity in the diagnosis of JRA. For follow up of disease progression, ultrasound and MRI are more sensitive than plain radiographs. Disease activity can be evaluated more accurately and complications can be detected earlier, potentially resulting in more effective treatment and improved outcomes.

REFERENCES

1. Miller M, Cassidy J. Juvenile rheumatoid arthritis. In : Nelson Text book of Pediatrics, 16th edition Philadelphia, Saunders,704-709
2. Wihlborg C, Babyn P, Marilyn R, et al (2001) Radiologic mimics of Juvenile rheumatoid arthritis. Pediatr Radiol 31:315-326
3. Johnson K, Gardner-Medwin J. Childhood arthritis: classification and radiology (2002) Clin Radiol 57:1;47-58
4. Cassidy JT, Martel W. Juvenile rheumatoid arthritis: clinicoradiologic correlations. (1977) Arthritis Rheum:20;207-211
5. Rosendahl K. Imaging of Arthritis in Children: Highlights of Pediatric Radiology : Syllabus 22nd postgraduate courseeuropean society of Pediatric Radiology 1999 May :64-67
6. Resnick D, Niwayama G. Osteoporosis. In: Resnick D.2nd edition. Philadelphia, Saunders, 1988:2022-2085
7. Lamer S, Sebag GH MRI and ultrasound in children with Juvenile chronic arthritis (2000) Eur J Radiol 33:2;85-93
8. Graham T, Blebea J, Gyllys-Morin V, et al (1997) Seminars in Arthritis and Rheumatism 27:3;161-168
9. Johnson K, Wittkop B, Haigh F, et al The early magnatic resonance imaging features of the knee in Juvenile Idiopathic Arthritis (2002) Clin Radiol 57:1;466-471
10. Gylys-Morin V, Graham T, Blebea J, et al (2001) Radiology 220:3;696-706
11. Keengwe I, Hegde S, Dearlove O, et al (1999) Anaesthesia 54(11) :1069-72

PLEUROPULMONARY BLASTOMA A RARE PRIMARY PULMONARY TUMOR OF CHILDHOOD

Preeyacha PACHARN, M.D.[1] Chantima RONGVIRIYAPANICH, M.D.[1]
Thomas J. BRYCE, M.D.[2] Suwannee SURATTANASOPHON , M.D.[1]

INTRODUCTION

Pulmonary neoplasms of all types are rare in children and pulmonary metastases are more common than primary tumors. Pleuropulmonary blastoma (PPB) is the least common malignant primary neoplasm. One quarter of cases occur in children and are often associated with congenital lung disease.[1,2]

PPB is a unique neoplasm of the lung and the pleura, containing both mesenchymal and/or epithelial elements that mimic the embryonal tissues of the developing lungs. Pediatric PPB differs from adult pulmonary blastoma in clinical presentation, gross and microscopic anatomical features, and outcomes. Patients usually have a poor prognosis and rarely survive more than 10 years.[3]

The clinical presentation is usually nonspecific. Symptoms and signs include respiratory difficulty, fever, chest pain and cough. Plain radiographs may demonstrate multicystic transformation of a lobe, pneumothorax, opacification of a hemithorax, pleural effusions, a pleural or diaphragmatic mass and shift of the mediastinum. Sometimes chest radiographs may simulate pleural effusion or empyema and fail to demonstrate a mass.

Two cases of pleuropulmonary blastoma are presented in this report.

CASE 1

A 3-year-old girl was referred from an outside hospital to our institution. She presented with high fever, chronic cough and anemia.

Chest radiograph at the outside hospital revealed a left pleural effusion. Thoracentesis yielded 800 cc of unclotted blood. A blood transfusion was performed, and the patient was transferred to our hospital.

On physical examination, the patient was tachypneic. There were decreased breath sounds on the left and decreased vocal resonance noted at the anterior left chest. Hepatomegaly was noted. Routine laboratory values were within normal limits.

A chest radiograph demonstrated near total opacification of the left hemithorax. (Figure 1)

CT scan showed a large cystic mass in the left hemithorax, measuring 9 x 6.5 cm in the axial plane. There were hyperdense areas within the mass which were thought to represent hemorrhage. Rim enhance-

[1] Department of Radiology Siriraj Hospital, Mahidol University 2 Prannok Road Bangkok Noi Bangkok Thailand 10700
[2] Department of Health Sociology Graduate School of Medicine of the University of Tokyo Bunkyoku Hongo 7-3-1 Tokyo, Japan 113-0033

ment was present. The mass compressed adjacent lung parenchyma and caused a slight shift of the mediastinum to the right (Figures 2a-d).

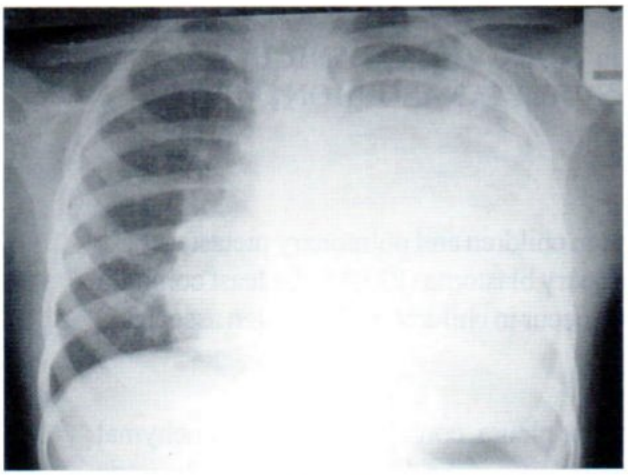

Fig.1 Chest radiograph of a 3-year-old girl (case 1) who presented with symptoms of respiratory tract infection. Near complete opacification of the left hemithorax is seen. A large left pleural effusion is suggested.

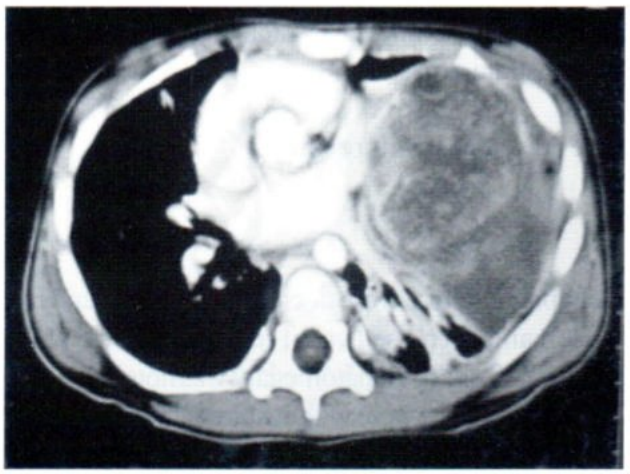

Fig.2A

Fig.2A-D Contrast-enhanced CT of the chest in case 1. There is a large cystic mass in the left hemithorax. There is compression of adjacent lung parenchyma and shift of the mediastinum.

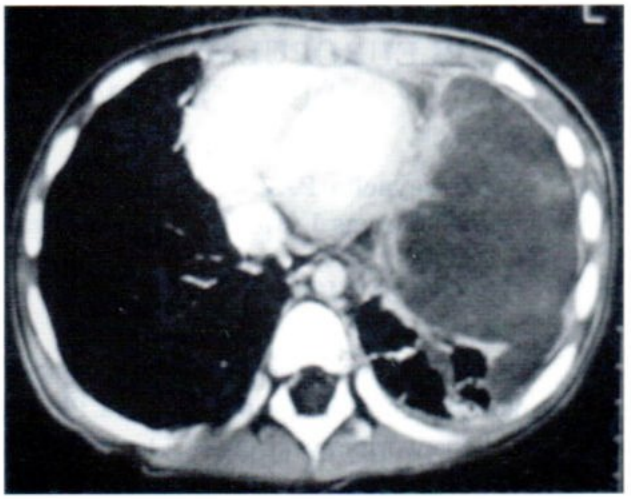

Fig.2B

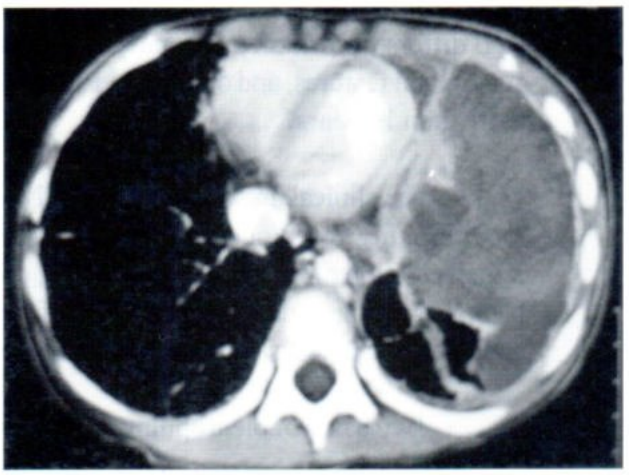

Fig.2C

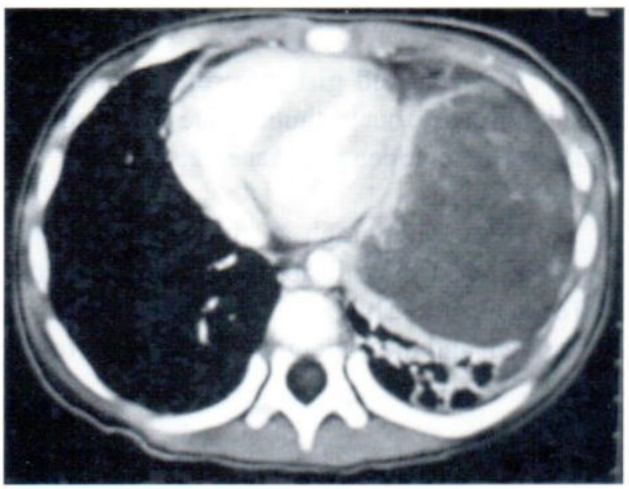

Fig.2D

CASE 2

A 4-year-old boy was referred to our institution from an outside hospital. He had presented with fever and dyspnea for 1 week.

A chest radiograph at the outside hospital showed a left lung mass. He underwent left thoracotomy with excision of the lung mass. Histologic findings were consistent with an embryonal rhabdomyo sarcoma with cartilageneous differentiation. He received postoperative chemotherapy. One week after chemotherapy, he developed a massive pleural effusion and was referred to our institution for further management.

Physical examination revealed a tachypneic patient. Breath sounds were decreased on the left. The abdomen was distended with no palpable mass. Routine laboratory values were within normal limits.

Chest radiograph showed opacification of the left hemithorax. There was marked mediastinal shift to the right. An underlying mass was felt to be likely. (Figure 3)

CT showed a large cystic mass with internal septations occupying the entire left hemithorax. The mass measured approximately 14 x 13 cm in the greatest axial dimensions. Herniation of the mass across the midline with shifting of the heart and mediastinal structures to the right was noted. (Figure 4a-c)

After contrast injection, peripheral and septal enhancement were demonstrated. (Figure 5a-c)

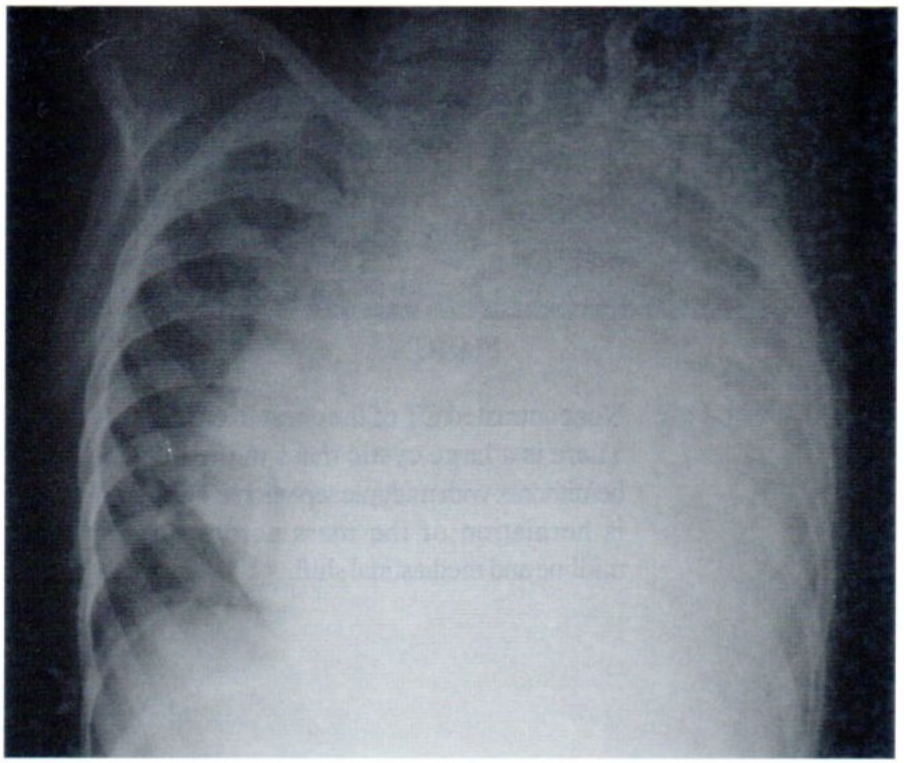

Fig.3 Chest radiograph of a 4-year-old boy (case 2). Opacification of the left hemithorax is seen with shift of the mediastinum to the right.

Fig.4A

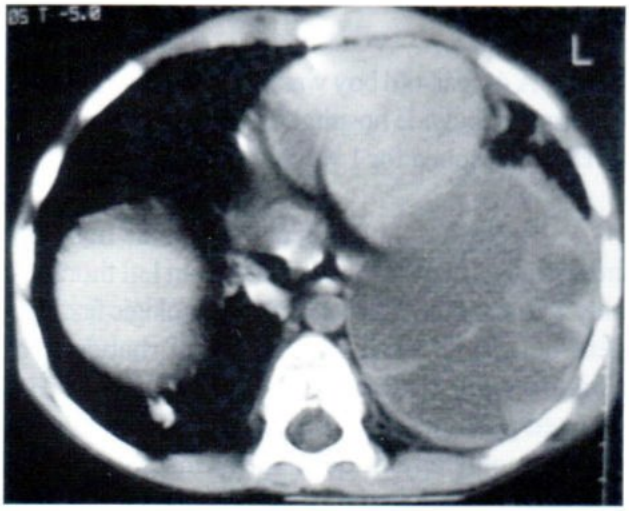

Fig.4B

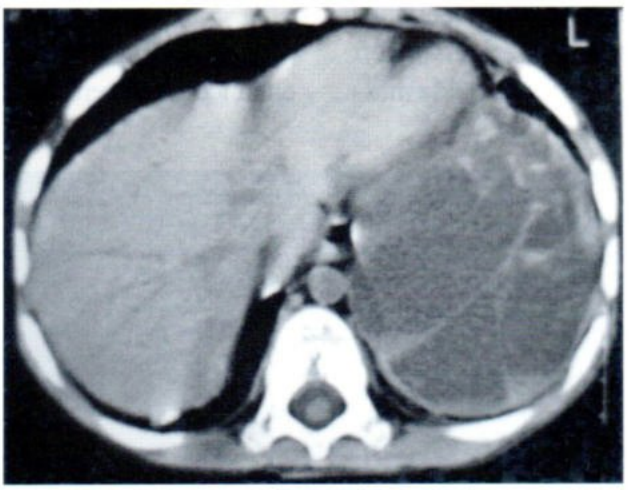

Fig.4C

Fig.4 a-c Noncontrasted CT of the chest in case 2. There is a large cystic mass in the left hemithorax with multiple septations. There is herniation of the mass across the midline and mediastinal shift.

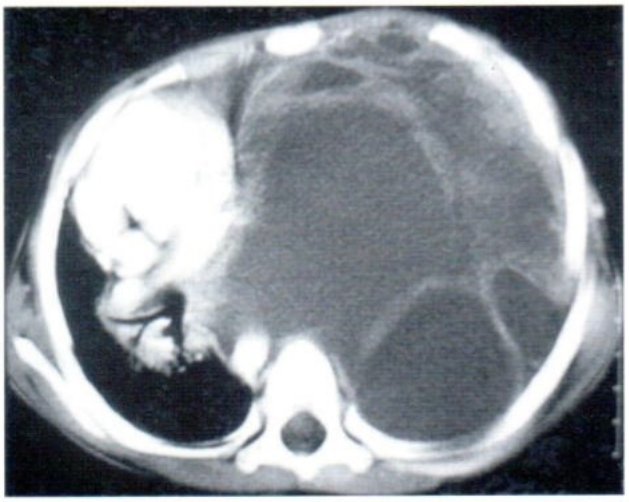

Fig.5A

Fig.5B

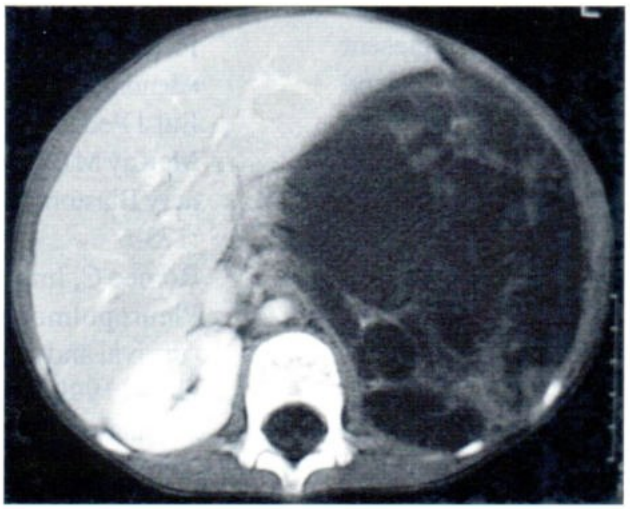

Fig.5C

Fig.5 a-c Contrast-enhanced CT in case 2 shows a mass with peripheral and septal enhancement

DISCUSSION

Plain radiographs in both of these cases showed near total opacification of the involved hemithorax. Such hemithoracic opacification with contralateral mediastinal shift could result from many causes such as a large pleural effusion or other space occupying mass. Consolidation alone usually does not cause marked mediastinal shift. In children presenting with respiratory symptoms and opacification of a hemithorax, a parapneumonic effusion should be considered. Pneumonia is the most common cause of pleural effusions in childhood. Other causes include congestive heart failure and renal failure. Malignancy is relatively rare in this age group.

If the etiology of a large pleural effusion appears fairly certain from history, physical examination and supporting laboratory data, thoracocentesis is usually avoided. Most patients recover without

having thoracotomy drainage.[4] However in complicated cases, pleural fluid analysis will help to identify the cause, and with large pleural effusion, thoracocentesis may be needed to relieve pressure in the affected hemithorax.

If patients fail to response to initial treatment, further investigation should be done. Ultrasound or computed tomography of the chest will help to determine whether the fluid is simple or complex, free-flowing or loculated, and identifying associated pathology such as an underlying mass lesion.

In our two cases, there were large cystic masses in the left hemithorax. No internal calcification was identified. In the first case, there was some internal hyperdensity which was thought likely to represent focal hemorrhage or a solid component. In the second case, internal septations were noted. Peripheral enhancement was demonstrated in both cases. According to these findings, an empyema could not be excluded. Due to the complexity of the visualized mass and the previous history of a histologically diagnosed tumor in case 2, a biopsy was performed. Biopsy results for both cases were consistent with pleuropulmonary blastoma (PPB).

Several cases of PPB have been previously reported.[5-8] Many of these cases involved cystic masses without a significant solid component. In such cases, approaching a specific diagnosis was very difficult and biopsy was necessary for definitive diagnosis.

Although the clinical and radiologic findings of this disease are not very specific, the histopathological appearance is quite distinctive, with a mixture of both epithelial and mesenchymal elements. PPB can be classified into three broad histologic categories.

Type 1 is purely cystic with smooth and glistening cyst linings. The adjacent pulmonary parenchyma is unremarkable. Twenty five percent of PPB is exclusively cystic.

Type 2 consists of multiple cysts and coalescing nodules with cystic degeneration, hemorrhage and necrosis.

Type 3 is a predominantly solid tumor with cystic areas only secondary to hemorrhage and necrosis.

In our two patients, surgical resection was performed and postoperative chemotherapy was administered. The tumors are classified in the type 2 category. These patients are still followed by pediatric oncologists at our institution.

REFERENCES

1. Federici S, Domenichelli V, Tani G, et. al. Pleuropulmonary blastoma in congenital cystic adenomatoid malformation: report of a case. Eur J Pediar Surg 2001, Jun;11(3) :196-9
2. McKay MJ, Yung T, Langlands AO. Pulmonary Blastoma. Clin Oncol 1990, May; 2(3) :173-6
3. Romeo C, Impellizzeri P, Grosso M, et. al. Pleuropulmonary Blastoma: Long term survival and literature review. Med Pediatr Oncol 1999, Oct;33(4) :372-6
4. Alkrinawi S, Chernick V. Pleural effusions in children. Semin Respir Infect. 1996 Sep;11 (3):148-54.
5. Perdikogianni C, Stiakaki E, Danilatou V, et al. Pleuropulmonary blastoma: an aggressive intrathoracic neoplasm of childhood. Pediatr Hematol Oncol. 2001 Jun;18(4):259-66.
6. Bini A, Ansaloni L, Grani G, et al. Pulmonary blastoma: report of two cases. Surg Today. 2001;31(5):438-42
7. Kukkady A, Upadhyay V, Pease PW, et. al. Pleuropulmonary blastoma: four cases. Pediatr Surg Int. 2000;16(8):595-8.
8. Merriman TE, Beasley SW, Chow CW. A rare tumor masquerading as an empyema: pleuropulmonary blastoma. Pediatr Pulmonol. 1996 Dec;22(6):408-11

THE PHANTOM STUDY OF SPATIAL REGISTRATION IN PET/CT

Taratip NARAWONG, MSc[1,2]; Kyosan YOSHIKAWA, PhD[1];
Kenji SAGOU, DDS[1];Katsumi TAMURA, MD[1]; Hiroyuki ISHIKAWA, MD[1];
Susumu KANDATSU, MD[1]; Kazutoshi SUZUKI, PhD[1];
Shuji TANADA, PhD[1]; Yasuhito SASAKI, PhD[1]; Hirohiko TSUJII, PhD[1]

ABSTRACT

Objective: The purpose of this study was to evaluate the spatial registration in terms of the registration difference in PET/CT with the phantom.

Method: Three experiments were performed by using the phantom insert with hollow spheres filled with F-18 and the combined PET/CT system(Siemens, Biograph), including the same offset correction(test 1,2,3) and varied offset correction for the gantry(offset 1,2,3), and the clinical setting. The location of the center of was used for statistical analysis of the location difference. A p-value less than 0.05 was defined to be statistically significant. The acceptable value for the registration difference in the registered image was taken as 1mm or less.

Result: The mean registration difference in the study of same offset correction for the gantry was 0.68±0.24 mm. The p-values obtained in the first experiment were more than 0.05. There was no statistically significant difference between each test. The average registration difference in the study of varied offset correction for the gantry was 0.51±0.17 mm. There was a statistically significant difference when the difference in the z-axis was more than 0.05 mm. The average registration difference in the clinical setting was 0.50±0.28 mm. There was no statistical significance between the clinical setting and the phantom setting.(p-value = 0.764)

Conclusion: In this PET/CT system, the spatial registration was sufficiently accurate in the phantom study and the spatial registration difference in the registered image was less than 1mm.

Key Words: PET/CT; F18; phantom; registration

[1] Research Center Hospital for Charged Particle Therapy, National Institute of Radiological Sciences, Chiba, JAPAN
[2] Division of Nuclear Medicine, Rajavithi Hospital, Bangkok, THAILAND

INTRODUCTION

Combined PET/CT systems are being used on an increasing scale in nuclear oncology. One important factor for using these systems is the accuracy of spatial registration between the PET and CT images. The accuracy of the registration between PET and CT depends on several factors such as the difference of the patient positioning, internal organ movements, attenuation correction artifacts and errors in the registration procedure.[1] Most studies on this subject have been performed in patients and have focused on internal organ movement especially respiration.[2-6] The lesion mislocalization can occur by the respiratory motion difference between PET and CT. It may be the major cause of the artifacts in PET/CT. This leads to a special breathing protocol in PET/CT study. A spatial registration study in a phantom was performed as part of a lung lesion study by a group of researchers in 2003.[7] The literature contains only a few reports on phantom studies in PET/CT. The purpose of this study was to evaluate the spatial registration difference in the registered image by using the phantom insert with hollow spheres.[8] This study relates to the system itself and to the effect of some parameters on the spatial registration difference between PET and CT in a phantom only.

MATERIALS AND METHODS

PET/CT system

The PET/CT system evaluated in this study was the BGO-based Siemens Biograph (Siemens Medical Systems, Inc). The Biograph combines a PET scanner (ECAT EXACT HR+) and a spiral CT (Somatom Emotion Duo) in a single gantry. The transverse fields of view of the PET and CT were 60 cm and 50 cm, respectively. The axial fields of view of the PET was 15.5 cm with 63 image planes per bed position (2.46 mm slice-to-slice spacing) Gantry offset was performed to ensure that the field of view of the system matches the PET and CT gantries. By acquiring the cross rod phantom, the gantry offset on the x, y and z axes is automatically calculated by the software. The offset in the x and y axes should be less than5 mm. The manufacture recommended that if either the x or y calibration values exceed 5 mm, mechanical re-adjustment of the gantries is required.

Phantom

The NEMA NU 2-2001(8) phantom insert with hollow spheres consists of six different diameters of sphere sizes i.e. 37±1 mm, 28±1 mm, 22±1 mm, 17±0.5 mm, 13±0.5 mm and 10±0.5 mm inserted in the cylinder water filled flood phantom. Each hollow sphere is filled with 0.185 MBq/cc of F-18.

The rod sources were used for gantry offset correction. Two Ge-68 rod sources with a radioactivity of about 148 MBq each were inserted in the box to make a cross rod phantom.

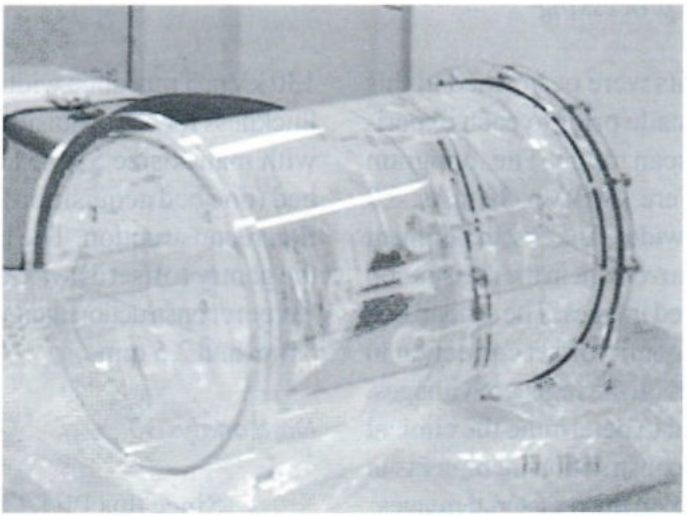

Fig. 1 Setting of NEMA NU 2-2001 phantom, inserting with hollow spheres, inserted in the water filled phantom.

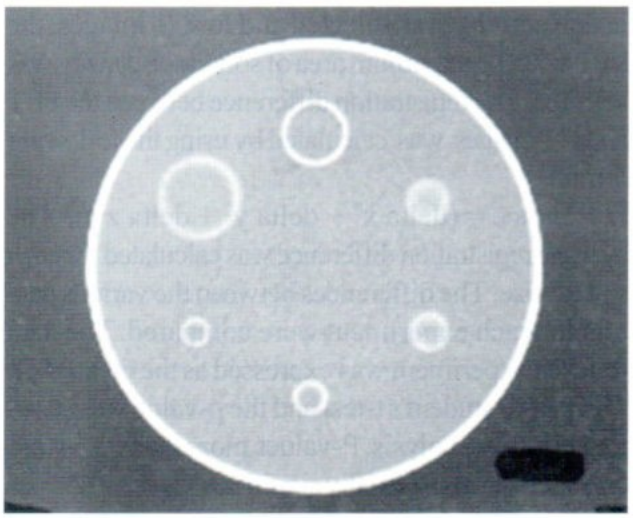

Fig. 2 CT image of the phantom with hollow spheres diameter ranging from 37 mm to 10 mm.

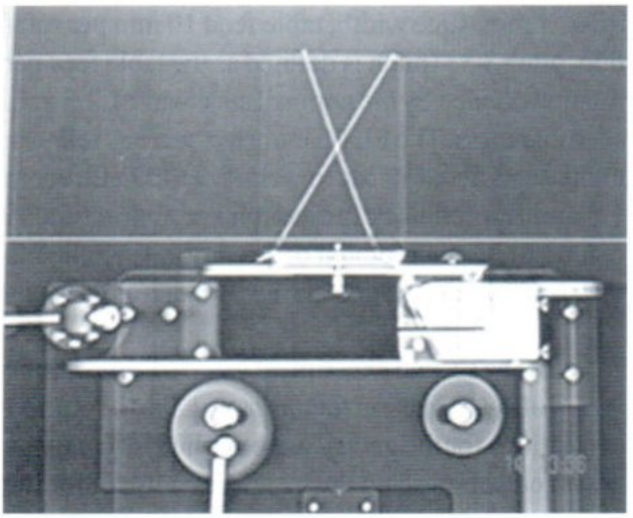

Fig. 3 Topogram of the cross rod phantom for gantry offset correction.

PET/CT acquisition and processing

Three experiments were performed in this study. The topogram is made prior to each experiment to define the axial scan range. The topogram acquisition parameters were 130 kVp, 30 mAs, 5.9 seconds and 1.0 mm slice width. The first experiment studied the effect of bed movement in the registration differences on the registered images. The second one investigated the effect of gantry offset correction in the registration differences on the registered images. The last one was designed to determine the clinical setting and the effect of reconstruction increments in the registration differences on the registered images.

The first experiment was performed using the same offset correction for the gantry. The experiment was repeated three times using the phantom with the bed in the reset position for each repeated experiment. CT acquisition was as followed: 130 kVp, 40 mAs, 3 mm. slice width, table feed 10 mm per rotation, pitch 3.33 (pitch is defined as the table feed per rotation divided by the nominal slice width), 2.5 mm. slice thickness. The PET parameters were as follows: total counts about 77 Mc, matrix size 512x512, zoom 1.0 and filtered back projection reconstruction. A reconstruction increment of 2.5 mm was applied to match the slice thickness of PET as much as possible.

The second experiment was performed using varied offset correction for the gantry. Two new offset corrections for the gantry were applied by using the cross rod sources and the standard protocol for the correction process. The phantom was acquired for each new offset correction for the gantry with the same system conditions. The phantom was acquired and reconstructed with the same parameter as for the first study and same PET scan time per bed. (15 minutes per bed and one bed acquisition) A reconstruction increment of 2.5 mm was used for the phantom data after the gantry offset correction had been applied.

The third experiment was performed with the usual clinical setting used in our institute i.e. 40 mAs, 130 kVp, 5 mm slice width, pitch 1.6 and 4mm slice thickness for CT acquisition. PET data was acquired with matrix size 512x512, zoom 1.92, 15 min per bed (one bed acquisition) and filtered back projection reconstruction. The latest offset correction for the gantry (offset 3) was applied in this experiment. Three reconstruction increments were used i.e. 5 mm, 4 mm and 2.5 mm.

Data analysis

Since this PET/CT was not equipped with software for analyzing the data generated in this study, all data had to be analyzed by using Dr. View/LINUX 1.1.0 software. All registered images were transferred to a snapshot format via CD-R. The sphere center was determined from several registered images. For PET images ,the slice with the maximum area of lesion activity was selected and for CT images, the slice with the maximum area of soft tissue density was selected. The registration difference between the PET and CT images was calculated by using the following formula [7]:

Difference = $(\text{delta } x^2 + \text{delta } y^2 + \text{delta } z^2)^{0.5}$ The average registration difference was calculated for each sphere size. The differences between the various data sets for each experiment were compared. The data for each experiment was expressed as the mean$\pm$SD. The paired student's t-test and the p-value were used for statistical analysis. P-values more than 0.05 were considered no statistically significant.

RESULTS

Three tests were done (test 1, 2 and 3) with the same phantom settings and the same offset correction for the gantry. After each test, the bed was reset to the normal position before starting the next test. This was necessary for checking the effect of bed movement on the registration difference in the registered images. The average registration difference for each sphere size was calculated and is shown in table 1.

TABLE 1 Average registration difference with same offset correction for the gantry

Sphere size (mm)	Average registration difference (mean±SD)(mm)		
	test 1	test 2	test 3
37	0.962±0.578	0.759±0.593	1.314±0.426
28	0.975±0.472	1.010±0.690	0.714±0.488
22	0.167±0.408	0.333±0.516	0.833±0.408
17	0.75±0.5	0.25±0.5	0.25±0.5
13	0.75±0.5	0.957±0.667	0.25±0.5
10	0.75±0.5	1.0±0	0.333±0.577

In the second experiment, the new offset correction for gantry was applied for each phantom experiment (offset 1, 2 and 3). Then the same analysis procedure was performed. This experiment was carried out for assessing the effect of gantry offset correction on the registration difference in the registered images. The average registration difference for each sphere size was calculated and is shown in table 2.

TABLE 2 Average registration difference with varied offset corrections for the gantry

Sphere size (mm)	Average registration difference (mean±SD)(mm)		
	offset 1	offset 2	offset 3
37	0.962±0.578	0.555±0.527	0.870±0.523
28	0.975±0.472	0.143±0.378	0.571±0.534
22	0.167±0.408	0.167±0.408	0.736±0.592
17	0.75±0.50	0.25±0.5	0.50±0.577
13	0.75±0.50	0	0.25±0.50
10	0.75±0.50	0.50±0.577	0.333±0.577

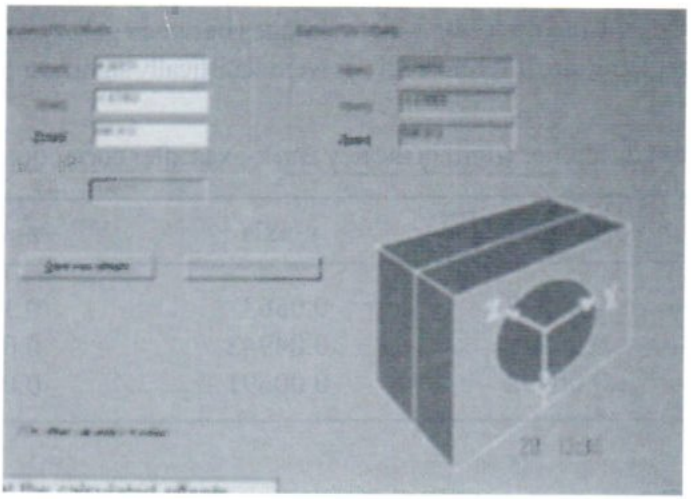

Fig. 4 Gantry offset calculation in the x, y and z-axes is carried out automatically by the software.

For the last experiment, clinical acquisition was performed and the data analyzed using the same procedure. This experiment was done to assess the effect of the reconstruction increment on the registration difference in the registered images when applied to the patient. This test was designed to determine intrinsic difference in PET/CT itself. It was not affected by body weight or internal organ movement. The average registration difference for each sphere size was calculated and is shown in table 3.

TABLE 3 Average registration difference using different reconstruction increments

Sphere size (mm)	Average registration difference (mean±SD) (mm)		
	5mm	4mm	2.5mm
37	0.883±0.525	0.833±0.408	0.667±0.50
28	0.603±0.717	0.25±0.50	0.916±0.432
22	0	0.667±0.577	0.667±0.516
17	0.50±0.707	0	0
13	0.50±0.707	0.333±0.577	0.25±0.50
10	0.50±0.707	0	0

DISCUSSION

In the first experiment the p-value for each test was more than 0.05(0.95 between tests 1and 2, 0.61 between tests 1and3 and 0.67 between tests 2 and 3) Bed movement in the z direction does not have any statistical significance. The variance for each test was calculated to estimate the reproducibility of the operator. The average variance in the PET and CT for the determination of the sphere center was less than 0.5mm. (0.44mm. for PET and 0.32 mm. for CT). The reproducibility of the operator was satisfactory. The average registration difference for all spheres and all tests was 0.686±0.238 mm. (mean±SD). This small number will not have any effect on the spatial registration in clinical practice.

The p-value in the second experiment with varied offset correction for the gantry was as follows: between offsets 1 and 2 it was 0.01, between offsets 1 and 3 it was 0.31 and between offsets 2 and 3 it was 0.04. The registration differences in the registered images between gantry offsets 1 and 2 and 2 and 3 were statistically significant.

TABLE 4 Gantry offset difference (mm) in the x, y and z-axes after correction

	x-axis	y-axis	z-axis
offset 1, 2	0.09427	0.0563	0.139
offset 1, 3	0.09919	0.04943	0.047
offset 2, 3	0.00492	0.00691	0.092

From table 4, it can be seen that the gantry offset difference between offsets 1 and 2 is smaller than between offsets 1 and 3 in the x-axis but larger in the y and z-axes. The gantry offset difference between offsets 2 and 3 is smaller than between offsets 1 and 3 in both the x and y-axes but larger in the z-axis. This implies that a difference in the z-axis has a greater effect than in the x and y-axes. This calls for caution regarding z-axis gantry offset correction. Though a certain statistically significant difference was found in this experiment, the average registration difference in the registered images for all gantry offsets was still less than 1 mm. (0.512 ± 0.167 mm.) The reproducibility of the operator is satisfactory with a small average variance in the PET and CT for the determination of the sphere center (0.36 mm. for PET and 0.29 mm. for CT)

The third experiment studied the effect of the clinical setting on the registration difference in the registered images as compared with the phantom setting. The p-value for the 5 mm reconstruction increment was 0.76. The different parameters in the clinical setting as compared with the previous data (offset 3) applying the same offset correction for the gantry does not show any effect on the registration difference in the registered images. When comparing the reconstruction increments of 5 mm, 4 mm and 2.5 mm, the p-value shows no statistically significant difference ($p>0.05$). The reconstruction increment does not have any effect on the registration difference in the registered images. Moreover, the average registration difference in the registered images for all three reconstruction increments was less than 0.5 mm. (0.420 ± 0.245 mm.) This means that for clinical acquisition, the reconstruction increment has no effect on spatial registration in the PET/CT as long as the reconstruction increment between PET and CT is numerically the same. The reproducibility of the operator was satisfactory since the average variance for PET and CT in the determination of the center of sphere was less than 0.5 mm.

From the three experiments used in this study, it can be seen that all data show a small spatial registration difference in the registered images in this PET/CT system. The manufacturer indicates that a registration difference in the registered image within 1 mm is acceptable. The results of this study thus substantiate that this system is satisfactory and the values obtained with it are acceptable even though there is a small registration difference in the registered images.

CONCLUSION

There is no statistically significant difference in terms of registration difference associated with bed movement in the z direction, the acquisition parameters such as the pitch number or CT slice thickness and the reconstruction increment. There is a statistically significant difference in the z direction and the gantry correction data and the gantry offset correction data but the difference is numerically less than 1 mm which is within the acceptable value.

ACKNOWLEDGEMENTS

The authors would like to thank Mr. Makoto Konno, Mr. Masaru Ohno and Mr. Takahiro Shiraishi for their generous support in the experiments. This study was performed under the Research project with Heavy Ions at NIRS-HIMAC,JAPAN.

REFERENCES

1. Vogel WV, Oyen WJG, Barentsz JO, Kaanders J H.A.M., Corstens F H.M. PET/CT: Panacea,Redundancy, or Something in Between? J Nucl Med 2004; 45: 15s-24s
2. Goerres GW, Kamel E, Heidelberg TNH, Schwitter MR, Burger C, Schulthess GK. PET-CT image co-registration in the thorax: influence of respiration. Eur J Nucl Med 2002; 29: 351-360

3. Goerres GW, Kamel E, Seifert B, et al. Accuracy of image coregistration of pulmonary lesions in patients with non-small cell lung cancer using an integrated PET/CT system. J Nucl Med 2002; 43: 1469-1475
4. Osman M, Cohade C, Nakamoto Y, Marshall LT, Leal JP, Wahl RL. Clinical significant inaccurate localization of lesions with PET CT: frequency in 300 patients. J Nucl Med 2003; 44: 240-243
5. Beyer T, Antoch G, Blodgett T, Freudenberg LF, Akhurst T, Mueller S. Dual-modality PET/CT imaging: the effect of respiratory motion on combined image quality in clinical oncology. Eur J Nucl Med Mol Imaging 2003; 30: 588-596
6. Nakamoto Y, Tatsumi M, Cohade C Osman M, Marshall LT, Wahl RL. Accuracy of image fusion of normal abdominal organs visualized with PET/CT. Eur J Nucl Med Mol Imaging 2003; 30: 597-602
7. Cohade C, Osman M, Marshall LT, Wahl RL. PET-CT: accuracy of PET and CT spatial registration of lung lesions. Eur J Nucl Med Mol Imaging 2003;30:721-726
8. NEMA. NEMA standards publication NU 2 -2001. Performance measurements of Positron Emission Tomographs. Rosslyn,VA: National Electrical Manufacturers Association; 2001: 30

DIAGNOSTIC ACCURACY OF THE MRI IN LUMBAR SPINAL STENOSIS AND LUMBAR DISK HERNIATION.

Bundhit TANTIWONGKOSI, MD[1] Pipat CHIEWVIT, MD[1]
Visit VAMVANIT, MD[2]

ABSTRACT

PURPOSE: To evaluate the diagnostic accuracy of MRI in lumbar spinal stenosis and disk herniation in symptomatic patients by using surgery as the comparison method.

MATERIALS AND METHODS: Sagittal T1-weighted, sagittal and axial T2-weighted MR images were obtained in 32 patients with lumbar spinal stenosis and 18 patients with lumbar disk herniation. All patients underwent surgery. The MR images were evaluated with regarding to intervertebral disk abnormalities, stenosis of the spinal canals, facet joint hypertrophy, ligamentum flavum hypertrophy and nerve root compression. The MR findings were compared with the surgical findings.

RESULTS: The accuracy of MRI in diagnosis of disk protrusion, extrusion, and sequestration was 89%, 83% and 89% respectively. Its diagnostic accuracy in detection of herniation location was 86%, 87%, and 89% respectively for central canal, centrolateral location and lateral recess. There was no negative surgical finding in this study. Nerve root compression was 80% accurately diagnosed by MRI. For the 11 cases in which disagreement between MRI and surgical findings, the breakdown was as follows. In 2 patients the MRI and diagnosis was that of disk protrusion but the surgical findings were those of extrusion. In one case, MR diagnosed disk extrusion but the surgery revealed a protruded disk. In one case, there was a sequestrated disk, while MR was interpreted as an extruded disk, and vice versa. About the location of herniation, MR was read as centrolateral location but the surgery showed only lateral location in one case. MR missed 2 cases of centrolateral disk herniation by being interpreted as lateral herniation. Concerning nerve root compression, MR over diagnosed one case of nerve root compression in a surgically proven nerve root deviation. However, MR missed one case of nerve root compression by being read as no compression. The accuracy of MRI in detection of central, centrolateral and lateral recess stenosis was 90%, 89%, and 83% respectively. Its diagnostic accuracy in facet joint hypertrophy, ligamentum flavum hypertrophy and nerve root compression was 83%, 84% and 82% in order. The disagreement between MRI interpretation and surgical findings did occur. Among these 10 patients, MRI showed one patient with centrolateral stenosis but surgery demonstrated only central canal stenosis, and vice versa. In one case, the facet joints were noted as unremarkable during surgery while MRI suggested hypertrophy. In contrary, MRI missed one case of surgically proven facet joint hypertrophy. In one case, MRI was read as ligamentum flavum hypertrophy, while surgery demonstrated normal size. MRI was not able to detect hypertrophy of ligamen-

[1] Department of Radiology, Siriraj Hospital, Mahidol University, 2 Prannok Rd., Bangkok, Thailand.
[2] Department of Orthopaedics, Siriraj Hospital, Mahidol University, 2 Prannok Rd., Bangkok, Thailand.

tum flavum in two cases. MRI over diagnosed one case of nerve root compression in a surgically proven normal nerve root while it missed one case of nerve root compression.

CONCLUSION: MRI is proven to be highly accurate in diagnosis of lumbar disk herniation and lumbar spinal stenosis. However, there is some disagreement on the diagnosis of disk protrusion, extrusion and sequestration; location of herniated disk, and lumbar stenosis; nerve root compression; facet joint hypertrophy and ligamentum flavum hypertrophy.

Low back pain is one of the leading causes of absence from work and disability.[1] Deyo et al[7] estimated that as many as 80% of all adults have low back pain at sometimes of their lives. Both lumbar spinal stenosis and lumbar disk herniation are the major causes of low back pain. A number of imaging methods are available for assessment of such abnormalities. MRI remains the noninvasive method of choice for assessment of the low back pain.[1] The sensitivity and specificity of MR imaging of intervertebral disk abnormalities are relatively well known.[1] However, there is less information about the value of MR imaging in the assessment of facet joints and ligamentum flavum.

The purpose of this study is to evaluate the diagnostic accuracy of MRI in lumbar spinal stenosis and disk herniation in symptomatic patients by using surgery as the comparison method.

MATERIALS AND METHODS

Patient Population

This cross-sectional study enrolled fifty patients with lumbar spinal stenosis or disk herniation who underwent lumbar spinal surgery at Department of Orthopaedics Surgery, Siriraj Hospital, Mahidol University during August- October, 2001. Written informed consent was obtained from all patients. The patients were operated on by the same orthopaedic surgeon (V.J.). All of them had lumbar MRI scanned before surgery.

32 patients had lumbar spinal stenosis, including 12 men and 20 women with 52-79 years old (mean, 61 years). 18 patients had lumbar disk herniation, including 13 men and 5 women with 28-54 years old (mean, 42 years).

The patients suffered from low back pain and/or radicular pain. The relevant clinical history and physical findings were collected. The patients with spinal tumor, infection or previous spinal surgery were excluded.

MR Imaging

The MR imaging was performed with a 1.5 -T ACS-NT scanner (Philips, Best, The Netherlands.) with a body coil. The protocol included sagittal T1-weighted (253/12 [repetition time msec/ echo time msec]) and T2-weighted (2588/120) turbo spin-echo imaging of the entire lumbar spines with the following sequence parameters: matrix, 256 X 180; field of view, 280 mm; section thickness 3 mm, intersection gap 0.5 mm. In addition, axial T2-weighted (3900/100) turbo spin-echo images of all lumbar intervertebral spaces (four sections per disc level from L1-S1) were obtained with the following sequence parameters: matrix, 256 X 210; field of view, 180 mm; section thickness, 4 mm; intersection gap, 0.5 mm.

Image Analysis

The imaging studies in all 50 patients were analyzed independently by one experienced neuroradiologist (P.C.). The three separate MR acquisitions were interpreted in the following manner. The sagittal T1-weighted images were evaluated for disk-space height; canal compression; presence and

configuration of epidural fat and nerve root in the neural foramina in the parasagittal plane; disk position and configuration; vertebral body signal; and upper lumbar neural canal, including the conus. The signal intensity of the disk and adjacent vertebral endplates were evaluated on T2-weighted sagittal image. In addition, the CSF-extradural interface was examined for the presence or absence of herniated disk and canal stenosis.

The presence of following abnormalities were recorded: spondylolisthesis, loss of normally high signal intensity of the disk on T2-weight image, loss of disk height, disk bulging, disk herniation (protrusion, extrusion and sequestration), thecal sac compression, nerve root compression, hypertrophy of facet joint, and hypertrophy of ligamentum flavum.

With regard to the disk abnormalities,[1] the following terms were used: normal, bulging, protrusion, extrusion, and sequestration.

Normal disk. The disk was considered to be normal when it did not reach beyond the borders of the adjacent vertebral bodies (Fig 1A).

Bulging disk. This diagnosis was made when a smooth, more or less circular extension of the disk margin was noted beyond the margins of the vertebral endplates. Bulging disk may be generalized, that was, be along the entire circumference of the vertebral endplate; in symmetric fashion with the smooth outline paralleling the contour of the vertebra endplate; or eccentric. Generally, a bulging disk was considered to be associated less with sciatica than disk herniation[3] (Fig 1B).

Disk protrusion. Protrusion was defined as a focal or asymmetric extension of the disk beyond the vertebral border, with the disk origin broader than any other dimension of the protrusion (Fig 1A).

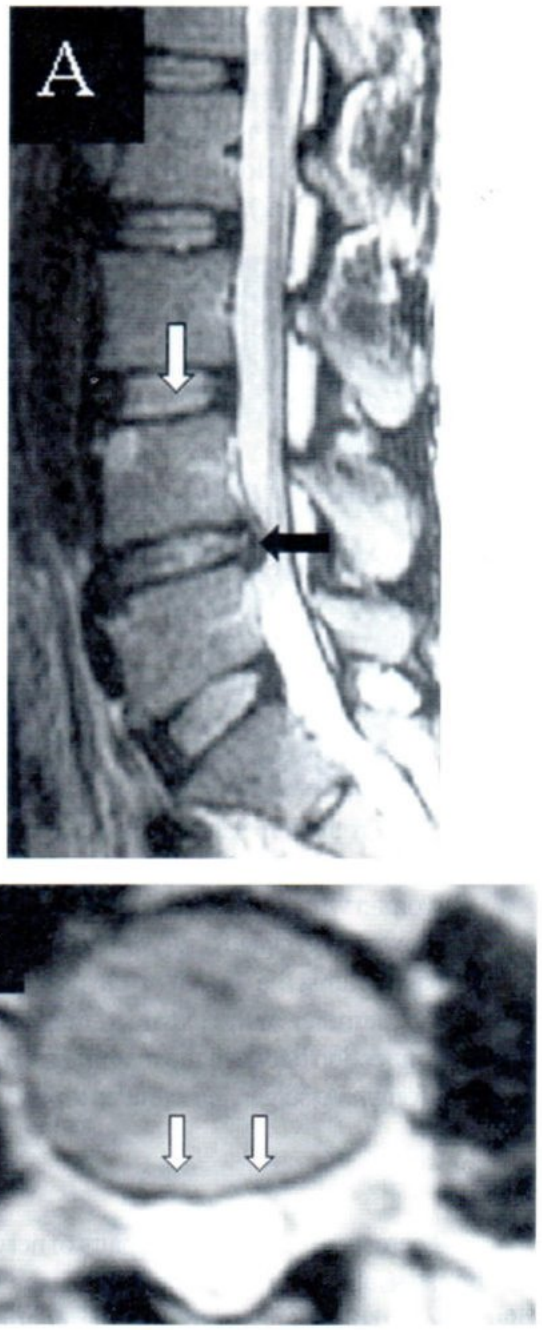

Fig. 1 Normal disk, bulging disk and disk protrusion. (**A**) Sagittal T2-weighted SE MR image of the lumbar spine in a 37 year-old man with low back pain showed normal L3-4 disk configuration (white arrow) and L4-5 disk protrusion (black arrow). (**B**) Axial T2-weighted SE MR image of the L3-4 intervertebral disk in another patient demonstrated a bulging disk (white arrow).

Disk extrusion. Extrusion was determined as a more extreme extension of the disk beyond the vertebral border, with the base against the disk of origin narrower than the diameter of the extruded material and a connection between the material and the disk of origin (Fig 2).

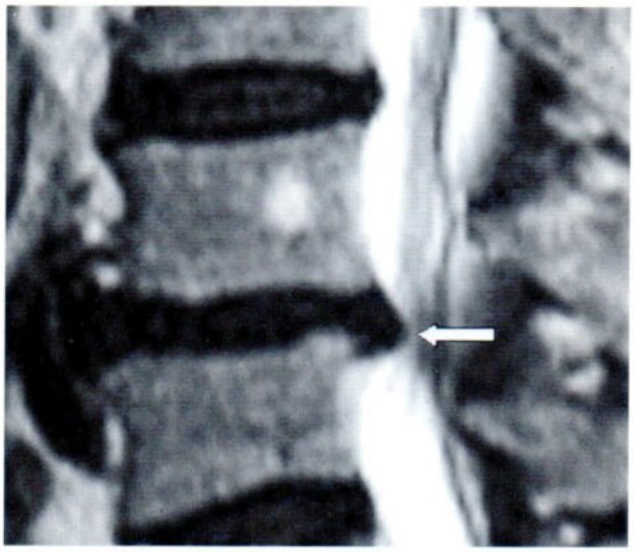

Fig. 2 Disk Protrusion. Sagittal T2-weighted SE MR image of the lumbar spine in a 28 year-old woman with low back pain and radicular pain showed a herniated disk(white arrow) with the base against the disk of origin narrower than the diameter of the extruded material and a connection between the material and the disk of origin. At surgery, an extruded disk was found.

Disk sequestration. Sequestration was defined as a free disk fragment that was distinct from the parent disk and had an intermediate signal intensity on T1-weighted images but an increased signal intensity on T2-weighted images (Fig 3).

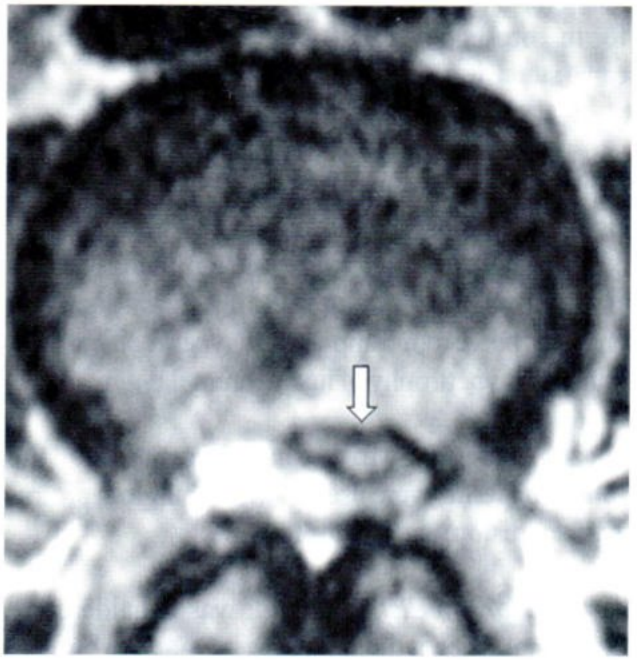

Fig.3 Disk sequestration. Axial T2-weighted SE MR image of the lumbar spine in a 40 year-old man with low back pain, severe radicular pain and positive straight leg raising test showed a free disk fragment (white arrow).

There were ordinarily two pairs of nerves that may be associated with the pathology of each lumbar intervertebral disk. These included descending and exiting nerves.[3]

Descending nerve. At each lumbar intervertebral disk, there was usually only one spinal nerve root outside the dural sac in the spinal canal descending behind the intervertebral disk to exit below the pedicle of the vertebral body forming the lower surface of the disk. At the L4-L5 intervertebral disk, for example, the descending nerve would be the L5 nerve root.

Exiting nerve. The exiting nerve was the nerve leaving the spinal canal through the top of the neural foramen below the pedicle of the vertebral body sitting on the top of the disk. At the L4-L5 disk, for example, the exiting nerve would be the L4 nerve, which usually left the dural sac at about the level of the lower part of the body of L3, descended behind the L3-L4 disk, and exited the spinal canal below the pedicle of L4 through the top of L4-L5 foramen.

The relationship of the nerve roots with the adjacent disks was described as no compression or

nerve root compression. An impression of thecal sac was diagnosed as either present or absent.

The endplates and adjacent bone marrow were graded according to the system of Modic et al [13] as follows: no abnormality, low signal intensity on T1-weighted images, and high signal intensity on T2-weighted images when compared to normal fatty bone marrow: type I, high signal intensity with both sequences: type II, and low signal intensity with both sequences: type III. When two different grades were present on both sides of intervertebral disk space, only one diagnosis was applied (first priority, type I; second priority, type II; last priority, type III).

Spinal canal. Spinal canal was divided in the axial plane into four zones: central canal zone, lateral recess or subarticular zone, foraminal zone and extraforaminal zone.[14] Criteria for spinal canal stenosis on MR images were 1) a distortion or paucity of epidural fat either in the neural foramina, lateral recess, or posteriorly between the ligamentum flavum (Fig 4), and 2) a diminution in the overall size of the neural foramina, neural canal, and/ or thecal sac. An attempt was made to determine the contribution of the hypertrophied facet joints and bony overgrowth as well as hypertrophy of ligamentum flavum.[4]

Facet joints. Facet joints were diathrodial joints formed by articulation of the superior articular process and inferior articular process. The shape and size of the facet joints were analyzed on axial images. The hypertrophy of facet joints[8] was defined as narrowing of the nerve root exit zones caused by superior or inferior facet bone growth (Fig 4). This did not include secondary causes such as an increase in the size of the capsuloligamentous (joint capsule) structures.

Ligamentum flavum. Ligamentum flava (Fig 4) were paired ligaments extending from the anteroinferior border of lamina above to the upper posterior border of the lamina below. The thickness of ligamentum flavum was measured on the axial plane at the level of spinal lamina. The normal value of its thickness on MR images was 5.54 mm ± 1.38.[8] It was considered hypertrophy if the ligament was larger than 6.92 mm (mean + 1SD).

The description and drawing of the surgical findings were recorded at conclusion of the surgery for each patient. The MR findings were compared with the surgical findings at the level of operation.

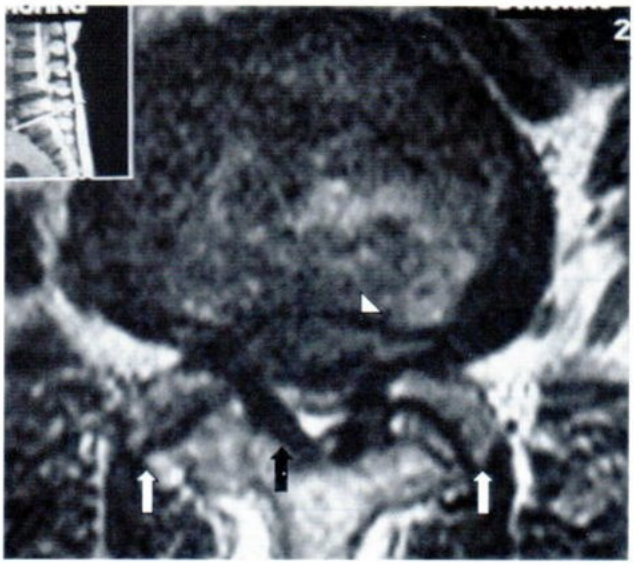

Fig.4 Axial T2-weighted SE MR image of the lumbar spine in a 68 year-old woman with low back pain, radicular pain relieved by squatting showed severe central canal stenosis due to facet joint hypertrophy (white arrow), ligametum flavum hypertrophy (black arrow) and herniated disk (white arrow head).

Statistical analysis

This study was a cross-sectional, diagnostic test. The sensitivity, specificity, positive predictive value, negative predictive value, accuracy and the 95% confidence interval of each parameter were calculated. The causes of disagreement between the MR findings and the surgical findings were analyzed.

RESULTS

Lumbar disk herniation

Table 1 listed the diagnostic values of MRI in lumbar disk herniation. These included sensitivity, specificity, positive predictive value, negative predictive value, accuracy and 95% confidence interval of each parameter.

Twenty disk explorations were performed in 18 patients. The accuracy of MRI in detection of disk protrusion, extrusion and sequestration was 89%, 83%, and 89% respectively. Its diagnostic accuracy in detection of herniation location is 86%, 87%, and 89% respectively for central canal, centrolateral location and lateral recess. There was no negative surgical finding in this study. Nerve root compression was 80% accurately diagnosed by MRI.

TABLE 1: Diagnostic Values of MRI in Lumbar Disk Herniation.

	Sensitivity (95% CI)	Specificity (95% CI)	PPV (95% CI)	NPV (95% CI)	Accuracy (95%CI)
Protrusion	75 (0.60,0.90)	93 (0.85,1.05)	75 (0.65,0.85)	89 (0.80,0.98)	89 (0.79,0.99)
Extrusion	83 (0.65,1.01)	83 (0.67,0.99)	71 (0.49,0.93)	91 (0.74,1.08)	83 (0.64,1.02)
Sequestration	86 (0.75,0.97)	90 (0.77,1.03)	86 (0.75,1.05)	90 (0.75,1.05)	89 (0.31,0.97)
Central	89 (0.76,1.02)	85 (0.73,0.97)	87 (0.70,0.99)	85 (0.71,0.99)	86 (0.74,0.98)
Centrolateral	83 (0.70,0.93)	91 (0.76,1.06)	85 (0.68,1.02)	88 (0.74,1.02)	87 (0.73,1.01)
Lateral recess	80 (0.61,0.99)	95 (0.82,1.02)	84 (0.75,1.01)	88 (0.75,1.01)	89 (0.75,1.03)
Nerve root compression	78 (0.63,0.93)	82 (0.68,0.96)	81 (0.64,0.99)	84 (0.65,1.03)	80 (0.67,0.93)

PPV = Positive Predictive Value, **NPV** = Negative Predictive Value

TABLE 2: Surgical and MR Results: Disagreement on Lumbar disk herniation.

MRI / Surgical Findings	Number of patients
Protrusion / Extrusion	2
Extrusion / Protrusion	1
Sequestration / Extrusion	1
Extrusion / Sequestration	1
Centrolateral / Lateral	1
Lateral / Centrolateral	2
Nerve root compression / Deviation	1
No compression / Nerve root compression	1
Total	11

Table 2 listed the disagreement between MR and the surgical findings. For the 11 cases in which disagreement between MRI and surgical findings, the breakdown was as follows. In 2 patients the MRI and diagnosis was that of disk protrusion but the surgical findings were those of extrusion. In one case, MR diagnosed disk extrusion but the surgery revealed a protruded disk. In one case, there was a sequestrated disk, while MR was interpreted as an extruded disk, and vice versa. About the location of herniation, MR was read as centrolateral location but the surgery showed only lateral location in one case. MR missed 2 cases of centrolateral disk herniation by being interpreted as lateral herniation. Concerning nerve root compression, MR over diagnosed one case of nerve root compression in a surgically-proven nerve root deviation. However, MR missed one case of nerve root compression by being read as no compression.

Lumbar spinal stenosis.

Table 3 listed the diagnostic values of MRI in lumbar spinal stenosis. These included sensitivity, specificity, positive predictive value, negative predictive value, accuracy and 95% confidence interval of each parameter.

TABLE 3: Diagnostic values of MRI in Lumbar Spinal Stenosis.

	Sensitivity (95% CI)	Specificity (95% CI)	PPV (95% CI)	NPV (95% CI)	Accuracy (95%CI)
Central	88 (0.74,1.02)	92 (0.85,0.99)	93 (0.86,1.04)	88 (0.79,0.97)	90 (0.82,0.98)
Centrolateral	83 (0.69,0.97)	91 (0.79,1.03)	78 (0.60,0.96)	90 (0.76,1.04)	89 (0.81,0.97)
Lateral recess	84 (0.72,0.96)	87 (0.72,1.02)	80 (0.75,0.95)	84 (0.68,1.00)	83 (0.65,1.01)
Facet joint hypertrophy	81 (0.69,0.93)	79 (0.62,0.96)	84 (0.71,0.97)	87 (0.72,1.02)	83 (0.68,0.98)
Ligamentum flavum hypertrophy	87 (0.70,1.04)	84 (0.70,0.98)	81 (0.64,0.99)	83 (0.65,1.01)	84 (0.70,0.98)
Nerve root hypertrophy	86 (0.74,0.98)	79 (0.61,0.97)	84 (0.76,1.02)	80 (0.75,0.95)	82 (0.68,0.96)

TABLE 4: Surgical and MR Results: Disagreement on Lumbar Spinal Stenosis.

MRI / Surgical Findings	Number of patients
Centrolateral / Central	1
Central / Centrolateral	1
Facet joint hypertrophy / Unremarkable	2
Unremarkable / Facet joint hypertrophy	1
Ligamentum flavum hypertrophy / Unremarkable	1
Unremarkable / Ligamentum flavum hypertrophy	2
Nerve root compression / Nerve deviation	1
No compression / Nerve root compression	1
Total	10

Forty decompressive laminectomies were performed in 32 patients with lumbar spinal stenosis. All operated levels were found stenotic as demonstrated by preoperative MR images.

The accuracy of MRI in detection of central, centrolateral and lateral recess stenosis was 90%, 89%, and 83% respectively. Its diagnostic accuracy in facet joint hypertrophy, ligamentum flavum hypertrophy and nerve root compression was 83%, 84% and 82% in order.

The disagreement between MRI interpretation and surgical findings did occur. Among these 10 patients, MRI showed one patient with centrolateral stenosis but surgery demonstrated only central canal stenosis, and vice versa. In one case, the facet joints were noted as unremarkable during surgery while MRI suggested hypertrophy.

On the contrary, MRI missed one case of surgically proven facet joint hypertrophy. In 1 case, MRI was read as ligamentum flavum hypertrophy, while surgery demonstrated normal size. MRI was not able to detect hypertrophy of ligamentum flavum in two cases. MRI over diagnosed one case of nerve root compression in a surgically-proven normal nerve root while it missed one case of nerve root compression.

DISCUSSION

MRI has been the imaging method of choice for evaluation of both lumbar disk herniation and lumbar spinal stenosis due to its high accuracy and noninvasiveness. Modic et al[4] found 82.3% agreement between MR and surgical findings for both types and location of disease.

Nevertheless, there was some disagreement between MRI and surgical findings that need to be clarified. These included disagreement on diagnosis of 1) disk protrusion, extrusion, and sequestration, 2) herniation or stenosis location, 3) nerve root compression, 4) facet joint hypertrophy, and 5) ligamentum flavum hypertrophy.

Disagreement on diagnosis of disk protrusion, extrusion and sequestration.

Both disk protrusion and extrusion can be found in asymptomatic volunteers but sequestration was rare in asymptomatic persons.[1] Boden et al[9] examined 67 asymptomatic individuals aged 20-80 years with MR images. They found at least 1 herniated disk in 20% of the individuals younger than 60 years and 36% of those older than 60 years. Jensen et al[10] reported that 98 asymptomatic individuals aged 20-80 years examined, 5% had disk bulging; 27%, protrusion; and 1%, extrusion of at least 1 disc level. Then distinction among protrusion, extrusion and sequestration was important since extrusion and sequestration seemed to cause symptoms.

In this study we used the morphologic characteristics to classify the type of herniated disks as previously mentioned in Imaging Analysis section. Disk extrusions were practically never seen at the disk level on axial sections. The large posterior displacement of the disc material beyond the margins of the intervertebral space still generally created images corresponding to the definition of a protrusion because they were outlined by the posterior longitudinal ligament. Significant migration of disk material was usually necessary to generate a typical extrusion at the disk level, was very often only possible on sagittal sections. Therefore it was sometimes confusing to diagnose either protrusion or extrusion by using morphological criteria.

Despite its apparent simplicity, only moderate interobserver and intraobserver agreement has been reported using this nomenclature in an independent study.[11]

Disagreement on diagnosis of herniation or stenosis location.

Distinction between the lateral recess stenosis and central canal stenosis was particularly important for the surgical management. A facetectomy may be necessary in addition to laminectomy and fusion in cases in which the lateral recess compromise was particularly severe.[6] Certainly, it was a little more unusual to encounter isolated lateral recess changes without some component of a central problem.

In this study we used the modified system proposed by Wiltse et al[5] in dividing the spinal canal into the central canal zone, lateral recess (subarticular zone), foraminal zone, and extraforaminal zone. The medial edge of the facet was the landmarks that separate the central zone from the subarticular zone. Unfortunately this landmark was generally not included in the axial sections at the disk level. Due to lack of visualized bony landmark on axial image, the boundary between the central and lateral recess was hard to be demarcated.

Disagreement on the diagnosis of nerve root compression.

Thornbury et al[7] suggested that adding the dimension of the nerve compression more directly impacts the treatment choice between surgical versus conservative therapy. In their study, the sensitivity of MRI in the diagnosis of disk-caused nerve compression was 91.9% and specificity is 52.4%. The low specificity implied that for MRI, the nerve root compression seem to be over diagnosed.

We found that two cases of nerve root compression were diagnosed by MRI while surgical findings revealed only nerve root deviation. All the deviated nerves in these cases were descending nerves in the thecal sac, which were more deviated or stretched rather than compressed. However, MRI missed 2 cases of surgically-proven nerve compression. The compressed nerves in these cases were exiting nerves at the foraminal zone. Retrospectively, the compressed nerves were better visualized by sagittal T2-weighted images in both cases, instead of axial views.

Disagreement on the diagnosis of facet joint hypertrophy.

Facet joint hypertrophy was a clinically significant factor of the low back pain especially when spondylolisthesis was present.[6] A single hypertrophic joint can encroach on two different nerve roots including the exiting part of the nerve root above and the descending part of the nerve root below.[5]

Weishaupt et al[1] found that mild and moderate osteoarthritis of facet joints was found in 18-22% in 60 normal volunteers; age 20-50 years. While no severe osteoarthritis was found in normal volunteers.

Our study used the increase in size of the facet joint as the criteria for diagnosing of facet joint hypertrophy. The evaluation seemed to be subjective since there was no standard reference for the average size of the normal facet joints. The discrepancy in diagnosis of facet joint hypertrophy was probably due to lack of standard size of reference and intraobserver bias.

Disagreement on the diagnosis of ligamentum flavum hypertrophy.

The bilateral ligamentum flava were the posterolateral boundaries of the spinal canal. Grenier et al[10] measured the thickness of the ligamentum flavum in axial plane at 49-53 levels in the 30 patients. The mean value was 5.54±1.38 mm. The thickness was greater than 6 mm at 14 levels. This reference value was probably greater than the actual mean value in asymptomatic Thai population.

The possible change in the thickness of ligamentum flavum dependent on load was studied in vitro by Schoenstroen and Hanssen.[5] and was found to be around 2 mm. In an already narrow spinal canal, a bulging inward of 2 mm from each side should severely affect the roots of the cauda equina, as has

been shown theoretically and experimentally.[5] A thickening of the ligamentum flavum in the cranial portion of the lateral recess could affect the descending segmental root.

Since our study used Grenier's mean value of normal ligamentum flavum thickness, this probably caused underestimation of the ligament thickness in 2 cases. Nevertheless, only minor discrepancy between MRI finding and surgical results was found.

Limitation

Although every effort was made to overcome limitations in this study, certain potential flaws became apparent. First, the population size was not large enough. To achieve higher accuracy with less allowable error, approximately 140 patients were needed. Second, intraobserver bias of both radiologist and orthopedic surgeon could make this study less accurate. To alleviate this bias, two or three experts were needed to interpret the images and the surgical findings. In case of disagreement, consensus should be made before final decision. Third, the intraobserver bias in diagnosis of facet joint hypertrophy still remained. A study of facet joint measurement in asymptomatic Thai individual was needed. Forth, the application of Grenier's mean value of normal ligamentum flavum thickness would not represent mean value of the ligament in Thai persons. Therefore we needed a study of ligamentum flavum measurement in asymptomatic Thai individuals.

CONCLUSION

MRI was proven to be highly accurate in diagnosis of lumbar disk herniation and lumbar spinal stenosis. However, there was some disagreement on diagnosis of disk protrusion, extrusion and sequestration; location of herniated disk, and lumbar stenosis; nerve root compression; facet joint hypertrophy and ligamentum flavum hypertrophy.

REFERENCE

1. Weishaupt D, Zanetti M, Hoilder J, Boos N. MR imaging of lumbar spine: prevalence of intervertebral disk extrusion and sequestration, nerve root compression, end plate abnormalities, and osteoarthritis of the facet joints in asymptomatic volunteers. Radiology 1998; 209(3): 661-666.
2. Kent D, Haynor D, Larson E, Deyo R, Diagnosis of lumbar spinal stenosis in adults: a metaanalysis of the accuracy of CT, MRand Myelography. AJR 1992; 158: 1135-1144.
3. Firooznia H, Benjamin V, Kricheff I, Rafii M, Golimbo C. CT of the lumbar spine disk herniation: Correlation with surgical findings. AJR 1984; 142: 587-592.
4. Modic M, Masaryk T, Boumphrey F, Goormastic M, Bell G. Lumbar herniated disk disease and canal stenosis: prospective evaluation by surface coil MRI, CT and Myelography. AJR 1986; 147: 757-765.
5. Wiltse L, Berger E, McCulloch A. A system for reporting the size and location of lesion in the spine. Spine 1997; 22: 1534-1537.
6. Brant-Zawadski M, Dennis S, Gade G, Weinstein M. What the clinician wants to know: low back pain. Radiology 2000; 217: 321-330.
7. Thornbury J, Fryback D, Turski P, Javid M, McDonald J, Beinlich B, et al. Disk-caused nerve root compression in patients with acute low back pain: diagnosis with MR, CT myelography and plain CT. Radioogy 1993; 186(3): 731-738.
8. Grenier N, Kressel H, SchieblerM, Grossman R, Dalinka, M. Normal and degenerative posterior spinal structures: MR imaging. Radiology 1987;165:517-525.

9. Boden D, Davis O, Dina S, Patronas J, Wiesel W. Abnormal magnetic resonance scans of the lumbar spine in asymptomatic subjects. J Bone Joint Surgery 1990; 72: 403-408.
10. Jensen C, Brant-Zawadski M, Obuchowski N, Modic M, Malkasian D, Ross J. Magnetic resonace imaging of lumbar spine in people without low back pain. N Eng J Med 1994; 331: 69-73.
11. Brant-Zawadski M, Jensen C, Obuchowski N. Interobserver and intraobserver variability in interpretation of lumbar disk abnormalities: A comparison of two nomenclatures. Spine 1995; 20: 1257-1263.
12. Schoenstroem N, Hansson T. Thickness of the Human Ligamentum Flavum as a function of load: An in vitro experimental study. Clin Biomechnics 1991; 6: 19-24.
13. Modic M, Masaryk T, Ross J, Carter J. Imaging of degenerative disk disease. Radiology 1988;168:177-186.

TITLE: PREVALENCE OF BREAST CANCER IN BI-RADS CATEGORY 3 LESIONS

Cholatip WIRATKAPUN M.D.[1], Yodying VASUTIT M.D.[2], Panuwat LERTSITHICHAI M.D.[2], Bussanee WIBULPHOLPRESERT M.D.[1]

ABSTRACT

Objective:

To determine the prevalence of breast cancer in patients found on mammography to have the Breast Imaging Report and Data System (BI-RADS) category 3 lesions.

Materials and methods:

1,704 women who underwent mammography during the one-year period from January 1st to December 31st 2001 were determined to have BI-RADS category 3 lesions. Of these, 1,100 had medical records available for review. Patients were included in the study if biopsies of the lesions were available, or if not, the followup time was at least two years. Presence of breast cancer was defined as cancer detected within two to three years after the initial mammogram at the site of the initial mammographic lesion. Patients not biopsied after two years were determined not to have breast cancer at the time of initial mammogram.

Results:

397 patients fulfilled the inclusion criteria. Biopsies were performed on 51 (12.8%) patients. Invasive breast cancer was found in two patients (2 of 397, 0.5%) and lobular carcinoma in situ in one.

Conclusion:

Our data suggest that the prevalence of breast cancer in patients with BI-RADS category 3 mammogram is extremely low (0.5%).

INTRODUCTION

The American College of Radiology has developed the Breast Imaging Reporting and Data System (BI-RADS), which is intended to standardize the terminology in the mammographic report, the assessment of the findings, and the recommendation of the action to be taken. " Probably benign finding" is the third of six numbered categories, used for categorizing lesions which are almost certainly benign, i.e., the risk of cancer is less than 2%. For these lesions, periodic mammographic surveillance is recommended

[1] Departments of Radiology
[2] Surgery Ramathibodi Hospital, Mahidol University, Rama 6th road, Bangkok 10400

as the preferred alternative to surgical or percutaneous biopsy, principally to avert morbidity and to reduce cost.[1-7]

The purpose of this study was to determine the prevalence of breast cancer in patients found on mammography to have BI-RADS category 3 lesions in Ramathibodi hospital.

MATERIAL AND METHODS

From January, 1st to December, 31st 2001, mammography was performed on 12,696 women at the breast diagnostic center, department of radiology, Ramathibodi hospital. In our practice, mammogram and subsequently ultrasound were performed in the same visit in all women. The final assessment was based on the combination of mammogram and ultrasound findings. Medical records and mammographic reports as well as sonographic reports of these patients were retrospectively reviewed. There were 1,704 women whose mammograms were classified as BI-RADS category 3 (13.4%). Patients were included in our study if they were followed for at least two years with mammography and/or sonography (if the lesions were invisible on mammograms), or if they underwent diagnostic fine-needle aspiration, core-needle biopsy or surgical biopsy. Exclusion criteria included cases which were not true category 3 lesions. For example, patients with negative findings on mammogram and ultrasound but had breast symptoms or had history of contralateral breast cancer or patients with typical category 2 lesions, were sometimes classified as category 3. Using these criteria, 397 patients were enrolled into this study. Age, history of contralateral breast cancer, presenting symptoms, physical examination, mammographic findings, corresponding sonographic findings, size of masses or complicated cysts and follow-up data were recorded. In the follow-up group, the lesions were compared to their appearances on last images and classified as stable, disappeared, progression and regression (when their sizes were smaller or the initial hypoechoic masses appeared as a simple cysts in the subsequently images.) Presence of breast cancer was defined as cancer detected within two to three years after the initial mammogram at the site of the initial mammographic lesion.

RESULT

Age of the patients ranged from 29-75 years old (median 49 years old). History of contralateral breast cancer was found in 34 cases (8.6%). Three hundred and nineteen patients (80%) had no breast symptoms. Sixty-three patients (15.9%) complained of palpable breast masses. Breast pain was noted in 12 patients (3%). Nipple discharge was found in three patients (0.8%). On breast examination, 350 cases (88%) had negative findings, while 47 cases (12%) had palpable masses. Mammographic findings are shown in table 1. Sonographic findings are shown in table 2. Size of masses or complicated cysts ranged from 0.3 -6 cm (mean 1 cm., S.D. 0.6). Fifty-one patients (12.8%) underwent tissue sampling for diagnosis. Benign pathologies were found in 48 patients. The reasons for intervention were surgeon's preference in 19 cases, progression of lesions in 14 cases and patient's request in 14 cases. For the follow-up group, the median imaging follow-up interval was 35 months (ranged 24-47 months). On last images, 50% of lesions were stable, 17% regressed, 5% progressed and 16% disappeared. We found two malignancies, which were invasive ductal carcinoma (stage T1N0M0) in one and invasive lobular carcinoma (stage T1N1M0) in another. The positive predictive value for malignancy in category 3 lesions was therefore 0.5%. One case of lobular carcinoma in situ (LCIS) was also found. This high-risk lesion was a serendipitous finding unrelated to imaged abnormality.[8,9] Details of cases with malignancy and lobular carcinoma in situ are listed in table 3.

TABLE 1: Mammographic findings

Findings	Number of cases	%
Mass	99	25
Calcifications	97	24.4
Asymmetric density	32	8
Architectural distortion	18	4.5
Mass containing calcifications	8	2
Abnormal axillary lymph node	4	1
Follow-up post excision, core-needle biopsy	4	1
Collapsed implants	1	0.3
Negative finding	134	33.7

TABLE 2: Sonographic findings

Findings	Number of cases	%
Mass	154	38.8
Complicated cyst	84	21
Mass containing calcifications	3	0.8
Abnormal axillary lymph node	3	0.8
Architectural distortion	2	0.5
Calcifications	1	0.3
Collapsed implants	1	0.3
Negative finding	149	37.5

TABLE 3: Details of cases with malignancies and lobular carcinoma in situ

Case	Age	Mammographic finding	Sonographic finding /size (cm.)	Reason for biopsy	Interval from diagnosis to biopsy (months)	Pathology
1	59	Asymmetric density	Solid nodule 0.7	Progression of lesion	12	IDC, T1N0M0
2	48	Negative	Solid nodule 0.7	Progression of lesion	30	ILC, T1N1M0
3	43	Mass	Solid nodule 1.2	Surgeon's preference	7	LCIS

Abbreviations: IDC = Invasive ductal carcinoma
ILC = Invasive lobular carcinoma
LCIS = Lobular carcinoma in situ

DISCUSSION

Mammography is accepted to be an effective screening method for breast cancer. Its wide use has resulted in the increase in the number of discoveries of small lesions, as well as microcalcifications, which are not palpable on the physical examination. Many lesions are judged to have a low probability of malignancy and can be periodically followed up. The basic purpose of this approach is to avert the morbidity and substantial cost of biopsies for benign lesions.[1-7] The three most common findings categorized as BI-RADS category 3 are (a) noncalcified solid masses with a round, oval, or gently lobular contour and margins that are predominantly circumscribed (b) clustered tiny round or oval calcifications and (c) focal asymmetric densities which partially thins on spot compression.[1,5] BI-RADS category 3 for ultrasound includes lesions which are solid masses with circumscribed margin, nonpalpable complicated cysts and clustered microcysts[1] The two most common mammographic findings which were classified as category 3 in our study were breast masses and calcifications, which were found in 25% and 24.4% of patients, respectively. The most frequently encountered abnormality seen by ultrasound was a breast mass, followed by complicated cyst.

The scientific evidence establishing the safety and efficacy of surveillance for BI-RADS category 3 lesions is based on many studies. Sickles[2] reported 17 out of 3,184 cases developed cancer (0.5%). According to two studies from Veras et al. in 1992[4] and 2002,[7] they found 9 out of 535 and 2 out of 511 patients had breast cancer (1.7% and 0.4%, respectively). Recently, Yasmeen et al. reported 30 patients with breast cancer from 2,927 category 3 cases (1%).[10] Our result, a prevalence of breast cancer of 0.5% (2 from 397 patients), was comparable to those of previous studies.

The surveillance protocol provided by the American College of Radiology is 6 month-interval follow-up for at least 2 or 3 years.[1] Interval progression of the lesions is prompt biopsy.[5] Progression of cancer during mammographic surveillance depends on the rate of growth or doubling time of an individual lesion. These values show great variation. Although rare, some cancers may grow so slowly that their size at mammography may not change for 1 or 2 years.[4,11] We also found an invasive lobular carcinoma which showed slow progression over 30 months.

Cancers initially considered to be "probably benign" eventually will be diagnosed early in their course, while they still have a favorable prognosis.[2,4,5,7]

In our study, there were one case of invasive ductal carcinoma, T1N0M0, compatible with stage I and one case of invasive lobular carcinoma, T1N1M0, compatible with stage IIA.[12] Both patients carried good prognosis. We found one LCIS, a high-risk lesions associated with an increased risk of malignancy in either breast. In general, it is not seen in both mammogram and ultrasound and is likely to be an incidental finding at excisional biopsy.[8,9]

LCIS = Lobular Carcinoma In Situ.

Ultrasound is a very useful adjunctive diagnostic tool for detecting abnormality, particularly in dense breasts, which significantly increased the sensitivity of mammography for cancer detection.[13] Ultrasound can differentiate solid from cystic lesions. Thus, mammographic apperance of a mass which is shown to be a simple cyst by subsequently ultrasound can be classified as category 2 with confidence. However, it can depict internal echo within the cysts, a finding termed complicated cysts, resulting in a classification as category 3. This may be the reason why there are many category 3 lesions in our practice.

Our study has several limitations. Firstly, there were high percentage of lost data due to unavailable medical records and many patients were lost to follow-up. Secondly, considerable variation exists among radiologists in the interpretation of the radiologic findings. More complete data collection, extensive follow-up, and standardization of interpretation of radiologic findings should lead to more accurate and reliable estimates of breast cancer prevalence in future studies.

CONCLUSION

Our data suggest that the prevalence of breast cancer in patients with BI-RADS category 3 is extremely low, i.e. 0.5%. All breast cancers found subsequently were early stage breast cancers.

REFERENCES

1. American college of radiology. Breast imaging reporting and data system (BI-RADS) 4th ED. Reston, Va: American college of radiology, 2003
2. Sickles EA. Periodic mammographic follow-up of probably benign lesions: results of 3,184 consecutive cases. Radiology 1991; 179:463-8
3. Orel SG, Kay N, Reynolds C, Sullivan DC. BI-RADS categorization as a predictor of malignancy. Radiology 1999;211:845-50
4. Veras X, Leborgne F, Leborgne JH. Nonpalpable, probably benign lesions:role of follow -up mammography. Radiology 1992; 184: 409-14
5. Sickles EA. Probably benign breast lesions: when should follow-up be recommended and what is the optimal follow-up protocol? Radiology 1999;213:11-4
6. Buchbinder SS, Leichter IS, Lederman RB, Novak B, Bamberger PN, Sklair-Levy M, et al. Computer-aided classification of BI -RADS category 3 breast lesions. Radiology 2004; 230: 820-3
7. Veras X, Leborgne JH, Leborgne F, Mezzera J, Janmandreu S, Leborgne F. Revisiting the mammographic follow-up of BI-RADS category 3 lesions. AJR 2002;179:691-5
8. Berg WA, Mrose HE, Loffe OB. Atypical lobular hyperplasia or lobular carcinoma in situ at core-needle breast biopsy. Radiology 2001; 218: 503-9
9. Foster MC, Helvie MA, Gregory NE, Rebner M, Nees AV, Paramakul C. Lobular carcinoma in situ or atypical lobular hyperplasia at core-needle biopsy: is excisional biopsy necessary? Radiology 2004; 231: 813-9
10. Yasmeen S, Romano PA, Pettinger M, Chlebowski RT, Robbins JA, Lane DS, Hendrix SL. Frequency and predictive value of a mammographic recommendation for short-interval follow-up. JNCI 2003; 95: 429-36

11. Kopan DB. Mammographic appearance of breast cancer. In:Kopan DB. Editors. Breast imaging.2nd ed. Philadelphia:Lippincott -Raven; 1997. p.375-408
12. Singletary SE, Allred C, Ashley P, Bassett LW, Berry D, Bland KI, et al. Revision of the American joint committee on cancer staging system for breast cancer. J Clin Oncol 2002; 20: 3628-36
13. Zonderland HM, Coerkamp EG, Hermans J, Van de Vijver MJ, Van Voorthuisen AD. Diagnostic of breast cancer: contribution of US as an adjunct to mammography. Radiology 1999; 213: 413-22

DIAGNOSTIC PERFORMANCE OF ULTRASONOMETER FOR EVALUATION OF OSTEOPOROSIS IN POSTMENOPAUSAL WOMEN

Somsri UARATANAWONG,[1] BSc. Somchai UARATANAWONG,[2] M.D.
Varodom BOONYAVISUT,[1] M.D.

ABSTRACT

Objects: To evaluate the diagnostic performance of quantitative ultrasound (QUS)
Study design: A diagnostic test (Cross-sectional descriptive study)
Methods: 324 postmenopausal women were evaluated for bone mineral density (BMD) at the lumbar spine and femoral neck by dual energy X-ray absorptiometry (DEXA) at Nuclear Medicine Division, Bangkok Metropolitan Administration and Vajira Hospital from January 2003–November 2004. BMDs were interpreted as osteoporosis by WHO criteria. The speed of sound (SOS) was also measured at the distal third of radius by quantitative ultrasound (QUS).
Results: The prevalence of osteoporosis in our study was 30.8%, sensitivity, specificity, positive predictive value, negative predictive value and positive likelihood ratio were 62%, 91.5%, 76.5%, 84.4% and 7 respectively.
Conclusion: SOS measurement at the distal third of radius by QUS had moderate sensitivity, but had high specificity when use DEXA as a gold standard and use WHO T-score as a reference. The highly specific test has been useful to confirm a diagnosis that has been suggested by other clinical data.

Key words: Osteoporosis, Dual energy X-ray absorptiometry, Quantitative ultrasound
Foot notes: **QUS** = Quantitative Ultrasound
DEXA = Dual Energy X-ray Absorptiometry
SOS = Speed of sound
BMD = Bone Mineral Density

Osteoporosis is systemic skeletal disease characterized by low bone mass and microarchitectural deterioration of bone tissue, with a consequent increase in bone fragility and susceptibility to fracture.[1] It is a significant cause of morbidity and mortality among postmenopausal women and has a major effect on the health economy worldwide.[2] Osteoporosis is a growing concern due to the increased in the percentage of aging in our population. It is therefore become imperative to evaluate and diagnose patients with osteoporosis so that preventive or therapeutic can be instituted as soon as possible.

The clinical management of osteoporosis relies heavily on the use of bone mass measurements, including quantitative computerized tomography, dual photon absorptiometry, radiographic absorptiometry, and dual-energy X-ray absorptiometry (DEXA). DEXA of the hip and spine has become the most widely accepted technique for evaluation of the skeleton status. DEXA measurements have good precision and accuracy, low radiation exposure, and are associated with hip and vertebral fracture risk.[3] However, owing to these machines require dedicated office space and can be expensive, they are not

[1] Nuclear Division, Department of Radiology, BMA Medical College and Vajira Hospital.
[2] Rheumatology Unit, Department of Medicine, BMA Medical College and Vajira Hospital

always accessible and tend to be located mainly in urban areas. To this end, several safe, precise, and accurate methods have been developed. The use of quantitative ultrasound (QUS) for the assessment of skeleton status has been to be a continued interest in recent years.[4-9] The attractiveness of QUS lies in its low cost, portability, ease of use, and freedom from ionizing radiation. It is possible that QUS may provide additional information on bone property (structure and strength) that is independent of BMD.[10-12] These benefits combined with preliminary clinical results showing good diagnostic sensitivity for fracture discrimination have encouraged further basic investigation.

There are essentially two approaches ultrasound assessment of bone: the first uses ultrasound velocity or speed of sound (SOS) and the second uses the frequency dependent attenuation. Ultrasound velocity is determined as the quotient of transit time and body part width or length and is quoted in meters per second (m/s), it is commonly measured at the calcaneus, tibia, patella, and phalanges. For frequency dependent attenuation, it is determined at the calcaneus. The attenuation parameter BUA is defined as the slope of attenuation versus frequency in this range and is reported in units of decibels per megahurtz. SOS and attenuation are both correlated with bone density and strength. Therefore, healthy bone will have a higher SOS and attenuation whereas osteoporotic bone will have a slower SOS and attenuation. In general, velocity is easier to measure and results in greater precision. Measurement of attenuation usually requires more complex hardware and results in less precised data.[4]

Recently, a quantitative ultrasound device that measures speed of sound (SOS) at multiple skeletal sites was introduced. Preliminary reports suggested that of the different skeletal sites measured by this device, the distal third of the radius is the preferred measurement site for osteoporosis.[13-14] In contrast to commomly used calcaneal QUS devices that evaluate ultrasound properties perpendicular to the load vector, determination of SOS along the radius seems more relevant to the mechanical load that is applied along the arm.

However, there is scarce studies in SOS measurement at the distal third of the radius. The aim of this study was to assess the diagnostic performance of quantitative ultrasound (SOS) at the distal third of the radius in detecting osteoporosis in Thai postmenopausal women using dual energy x-ray absorptiometry as the gold standard.

SUBJECTS AND METHODS

Subjects

The study included 324 Thai postmenopausal women who attended Bangkok Metopolitan Administration and Vajira Hospital from January 2003 to November 2004. The study has been approved by the Medical Ethics Committee of Bangkok Metropolitan Administration, and written informed consent is obtained from participants. Baseline data consist of both demographic and clinical variables such as age, height, weight, date of the last priod and duration of postmenopause. Postmenopausal duration was the period after the final menstrual period regardless of whether it was spontaneous or induced, that was duration of current age in years minus age at menopause. Menopause was indicated after 12 consecutive months of amenorrhea, regardless of pathological or physiological cause. The study subject consisted of two groups, osteoporotic and non-osteoporotic. The osteoporotic group (n=100) was comprised of postmenopausal females with a BMD more than 2.5 standard deviations (SD) below the mean young normal bone mass (T-score) at the lumbar spine and/or femoral neck as determined by the Lunar normative database. Vital signs, height, and weight were

BMD = Bone Mineral Density, **BUA** = Broad band Ultrasound Attenuation, **SOS** = Speed of Sound, **SD** = Standard Diviation, **QUS** = Quantitative Ultrasound

collected. Subjects who met all inclusion and exclusion criteria underwent a DEXA scan of the hip and posteroanterior spine and quantitative ultrasound (SOS) of the left distal third of the radius.

Exclusion criteria included diseases or conditions known to affect bone health, including chronic kidney disease, long-term immobilization, smoking, and medications (fluoride, calcitonin, bisphosphonates, corticosteroids, thiazides, anticoagulants). Appropriate informed consent forms were obtained from every subject. Each postmenopausal women was undergone both DEXA and QUS measurements by independent radiological technologist.

Quantitative ultrasound (bone sonometry)

Measurements of the velocity of the ultrasound wave, expressed as speed of sound (SOS) in m/s, were done using quantitative ultrasound (The Sunlight Omnisense™ 7000S Bone sonometer device, Israel) at distal third of radius. It is designed to measure SOS of ultrasonic waves axially transmitted along bones. The ultrasound wave are conducted along the bone and then detected by two different transducers assembled within the probe. By measuring the propagation times along the different trajectories, originating at one of the transmitting transducers and arriving at one of the receiving transducers, the SOS of the bone is determined. The non-dominant side was uniformly used for examination, left usually, unless a history of fracture was present. Each value recorded was the mean of 3 consecutive determinations. The total scanning time with analysis took no more than 5 minutes.

QUS quality controls suggested by the manufacturer were carried out daily before the examinations. To quantify the precision error of this instrument, the instrument precision underwent a total of three measurements without repositioning in 18 subjects. The repositioning/interobserver precision underwent a total of three measurements of each in the same day by three technologists. The short term precision underwent one measurement on 5 separate days within one week period in 10 subjects. The instrument precision was 0.47%. The interobserver precision was 0.38-0.47%. The short term precision was 0.43%.

Dual energy x-ray absorptiometric measurements

Bone mineral measurements with DEXA were performed with a bone densitometer with a Lunar DPX-L (Lunar Radiation Corporation, Madison, WI, USA) at the lumbar spine (L2-L4) and the left proximal femur (femoral neck). The machine was calibrated daily using a quality assurance phantom. The precision error of the technique expressed as CV was 0.5% for the lumbar spine phantom and 1.3% for the hip phantom.

To ascertain whether the SOS values could identify osteoporotic and non-osteoporotic groups, the SOS mean and standard deviation were calculated for each group. Comparison between groups was made using an unpaired two-tailed Student's t-test. The Pearson correlation coefficients were calculated for weight, BMI, SOS, lumbar spine BMD and proximal femoral BMD. Data are expressed as mean ±SD. A p value < 0.05 was considered statistically significant.

DEXA = Dual energy X-ray Absorptiometry, **SOS** = Speed of Sound, **QUS** = Quantitative Ultrasound, **CV** = Coeffieient of Variation, **BMI** = Body Mass Index

RESULTS

TABLE 1 Demographic of study population (n=324) (mean±SD, range)

Age (years)	59.6±10.19	39 to 97
Years since menopause	10.7±8.96	1 to 50
Age at menopause	48.9±3.06	33 to 55
Body weight (Kg)	55.7±9.28	32 to 92
Height (cm)	152.1±8.19	152 to172
Body mass index (Kg/m^2)	23.9±3.79	16 to 40.3
L-spine BMD (g/cm^2)	0.980±0.19	0.959 to 1.002
L-spine BMD (T-score)	-1.163±1.59	-1.347 to -0.993
FN BMD (g/cm^2)	0.645±0.66	0.572 to 0.718
FN BMD (T-score)	-1.169±1.25	-1.312to -1.034
Left forearm SOS (m/s)	4043.39±157.13	3658 to 4468
Left forearm T-score	-1.255±1.37	-1.406 to -1.105

TABLE 2 WHO criteria for lumbar spine/ Femoral neck BMD

	Non-osteoporosis (n=224) T-score ≥ -2.5	Osteoporosis (n=100) T-score < -2.5	p-value
Age (years)	56.1±7.73	67.2±10.39	<0.001
Years since menopause	7.8±6.86	17.4±9.56	<0.001
Age at menopause	48.3±3.02	50.3±2.68	<0.001
Body weight (Kg)	57.4±9.11	51.3±5.7	<0.001
Body mass index (Kg/m^2)	24.3±3.82	23.2±4.29	<0.05
L- spine BMD (g/cm^2)	1.064±0.16	0.788±0.11	<0.001
L- spine BMD (T-score)	-0.46±1.51	-2.75 ±0.91	<0.001
FN BMD	0.824±0.122	0.611±9.72	<0.001
FN BMD (T-score)	-0.634 ±1.00	-2.371 ±0.86	<0.001
Left forearm SOS (m/s)	4099±124	3919±151	<0.001
Left forearm (T-score)	0.77±1.08	-2.34±1.34	<0.001

Values are the mean±SD, LS= lumbar spine; FN= femoral neck; BMD= bone mineral density

DEXA = Dual Energy X-ray Absorptionretry, **QUS** = Quantitative Ultrasound, **FN** = Fermoral Neek
SOS (m/s) = Speed of Sound (meter/sec), **CV** = Coeffieient of Variation, **BMI** = Body Mass Index

TABLE 3 The characteristics of diagnostic performance taking QUS and DEXA-BMD

QUS (Test)	DEXA		Total
	T-score<-2.5	T-score>-2.5	
T-score<-2.5	62	19	81
T-score>-2.5	38	205	243
Total	100	224	324

QUS = Ouantitative Ultrasound
DEXA = Dual energy X-ray Absorptiometry
FN = Femoral neek

TABLE 4 Correlation coefficients between age, body weight, BMI, LS and FN BMD, and wrist SOS

		Age	Meno dura	Wt	BMI	Wr-SOS	BMD_FN	BMD-LS
Wr-SOS	Pearson Correlation	-.507*	-.466*	.105	.007	1.000	.068	.527*
	Sig. (2-tailed)	.000	.000	.059	.898	.	.225	.000
	N	322	322	322	322	322	318	321
BMD-FN	Pearson Correlation	-.115	-.070	.225	.209	.068	1.000	.363
	Sig. (2-tailed)	.039	.214	.000	.000	.225	.	.000
	N	320	320	320	320	318	320	318
BMD-LS	Pearson Correlation	-.454*	-.450*	.378	.222	.527	.363*	1.000
	Sig. (2-tailed)	.000	.000	.000	.000	.000	.000	.
	N	322	322	322	322	321	318	322
Wt	Pearson Correlation	-.243	-.248	1.000	.874	.105	.225	.378
	Sig. (2-tailed)	.000	.000	.	.000	.059	.000	.000
	N	324	324	324	324	322	320	322
BMI	Pearson Correlation	-.048	-.047	.874	1.000	.007	.209	.222
	Sig. (2-tailed)	.387	.403	.000	.	.898	.000	.000
	N	324	324	324	324	322	320	322

* Correlation is significant at the 0.05 level (2-tailed).
Meno dura = duration of menopause, Wt= weight, BMD=bone mineral density, LS=lumbar spine, FN=femoral neck, BMI=body mass index, Wr = Wrist

A total of 324 postmenopausal women in Bangkok Metropolitan Administration Medical College and Vajira Hospital were participated. As shown in Table 1, their average age, BMI, age at menopause, duration of menopause, lumbar spine and femoral neck BMD, and SOS at the wrist, were 59.6 years, 23.9, 48.9 years, 10.7 years, 0.980±0.96 g/m^2, 0.645±0.57 g/m^2 and 4043m/sec respectively.

As displayed in Table 2, the women were classified by the WHO criteria for BMD at the lumbar spine and/or femoral neck to non-osteoporosis and osteoporosis. There were significant differences among the groups in term of age, years since menopause, age at menopause, BMI, SOS and BMD at the lumbar spine and femoral neck.

BMDs were measured in 324 postmenopausal women by DEXA as a gold standard and by QUS measurement as a new diagnostic test. The prevalence of osteoporosis was 30.8%. False positive rate is 8.4%, and false negative rate is 38%. The sensitivity of QUS using DEXA as the gold standard was moderate (62%) but had high specificity (91.5%). The probability that the subjects with a positive test result would have the osteoporosis (positive predictive value) was 76.5% and the probability that an individual with a negative test result would not have the osteoporosis (negative predictive value) was 84.4%. The chance of test positive if the subject has disease (LR+) is 7 times to the chance of a positive result if the subjects do not have disease (Table 3).

Correlation coefficients for BMD and SOS between different anatomic sites are shown in Table 4.Lumbar spine and femoral neck BMD had a correlation of 0.363. SOS correlated better with lumbar spine BMD (0.527) than with femoral neck BMD. Both age and duration of menopause were negatively correlated with SOS (-0.507 and -0.466) and lumbar BMD (-0.454 and –0.450).

DISCUSSION

Much less has been published about QUS (SOS) at the distal third of the radius.

In our study, SOS and BMDs (lumbar spine and femoral neck) have been shown to be significantly decreased in women with osteoporosis which compatible with many studies.[14-16] Our results are similar to study of Weiss et al[14] who used the same method and site.

The objective of this study is to determine the diagnostic performance of QUS (SOS) radius measurement in the case finding of osteoporosis in postmenopausal women using DEXA as gold standard. To assess the diagnostic performance, we use the accuracy of the test, which is the correspondence with sensitivity and specificity. In this study we found that QUS at the distal third of radius had a moderate sensitivity (62%) for predicting BMD- osteoporosis, but had a high specificity (91.5%). In study of Benitez CL et al,[16] the sensitivity and specificity were 84% and 50% respectively. They studied QUS (SOS) at the proximal phalanxes in 206 postmenopausal Mexican-American women. Massie A et al[17] found that only 44% of the perimenopausal women whose spinal DEXA falls within the lowest quartile being in the lowest quartile of BUA of the calcaneus. Difference in results might be from population, measurement technique and site. In our study the high specific test (QUS) has been useful to confirm (rule in) a diagnosis that has been suggested by other clinical data. This is because highly specific test is rarely positive in the absence of disease - that is, it gives low false positive results. Therefore, DEXA examination could be avoided if procedure with QUS is performed at the beginning of a diagnostic work-up. In this study positive predictive value (76.5 %) was relatively low for QUS as a predictor of BMD -defined osteoporosis. This might be because of a test with high specificity (low false positive among the

BMD = Bone Mineral Density, **SOS** = Speed of Sound, **DEXA** = Dual energy X-ray Absorptionretry, **(LR+)** = positive Lihulthood Ratio

disease free) could have low positive predictive value if the ratio of disease-free to disease subjects was high.[18]

The likelihood ratio for a particular ratio of a diagnostic test is defined as the probability of that test result in people with disease divided by the probability of the result in people without disease. Likelihood expresses how many times more (less) likely a test reszult is to be found in disease compared with non-disease people.[18] In this study the positive likelihood ratio was 7.0 which meant that a subject with positive test was 7 times more likely to occur osteoporosis than one without it. A high likelihood ratio for a positive result has shown that the test (QUS) provided useful information.

The correlation of radius QUS and DEXA at the lumbar spine was modest (0.53) and was better than at the femoral neck. One of the reasons for different correlation between sites is probably bone composition. The correlation between QUS and BMD measurements has been examined in several studies. Depending on the population studied, method (SOS or BUA) and the site of measurement (calcaneus, radius, phalanx), correlation was ranged from 0.29 to 0.90.[15,17,19-21]

DEXA is presently the standard method for assessing BMD. The technique provides an apparent area density (BMD) calculated as bone mineral content /bone area and expresses density as g/cm^2, therefore the standard DEXA technique measures not true bone mineral density (g/cm^3), but rather areal density(g/cm^2). In contrast to bone density measurements, QUS which is mechanical wave may have greater potential to assess of three dimensional structure and strength.[12] This advantage is especially significant for some chronic (rheumatic) disorders associated with bone growth; when comparing 2 bones of different sizes but with the same mineral content, the larger will show artificially higher BMD than the smaller one. Thus, QUS appeared to be less dependent on anthropometric parameters.

In conclusion, our study was a cross-sectional study on a postmenopausal population that needs to be further validated with larger groups. However, promising results were seen in the application of radius QUS as to confirm (rule in) a diagnosis of osteoporosis that has been suggested by other clinical data. The application of QUS will help to prevent unnecessary DEXA. A low cost, portable and radiation-free screening tool would also be beneficial for the assessment of the skeletal status in much of the population.

ACKNOWLEDGMENTS

The authors wish to thank the Vajira Medical Research Fund, Bangkok Metropolitan Administration Medical College and Vajira Hospital for a grant.

REFERENCES

1. Anonymous 1993 Consensus Development Conference: Diagnosis, prophylaxis, and treatment of osteoporosis. Am J Med 1993; 94:646-50.
2. Cooper C,Campion G, Melton LJ. Hip fractures in the elderly: worldwide projection. Osteoporos Int 1992;2: 258-89.
3. Kellie SE. Diagnostic and therapeutic technology assessment (DATTA). JAMA 1992; 267: 286-8, 290-4.
4. Njeh CF, Boivin CM, Langton CM. The role of ultrasound in the assessment of osteoporosis: a review. Osteoporosis Int 1997;7:7-22.
5. Gluer CC. Quantitative ultrasound techniques for the assessment of osteoporosis: expert agreement on current status. J Bone Miner Res 1997; 12: 1280-8.

BUA = Broad band Ultrasound Attennation, **SOS** = Speed of Sound

6. Greenspan SL, Bouxsein Ml, Melton ME, Kolodny AH,Clair JH, Delucca PT, et al. Pricision and discriminatory ability of calcaneal bone assessment technologies. J Bone Miner Res 1997 ;12:1303-14
7. Kaufman JJ, Einhorn TA. Perspectives ultrasound assessment of bone.J Bone Miner Res 1993;8:517-25
8. Brunader R, Shelton DK. Radiologic bone assessment in the evaluation of osteoporosis. Am Fam Physician 2002;1:1357-64.
9. Daragon A, Krzanowska K, Vittecoq O, Menard JF, Hau I, Jouen-Beades F,et al. Prospective X-ray densitometry and ultrasonography study of the hand bones of patients with rheumatoid arthritis of recent onset. Joint Bone Spine 2001; 68:34-42
10. Gluer CC, Wu CY, Genant HK. Broadband ultrasound attenuation signals depend on trabucular orientation: An vitro study. Osteoporosis Int 1993; 3: 185-91.
11. Takano Y, Turner CH, Burr DB. Mineral anisotropy in mineralized tissues is similar along spices and mineral growth occurs independent of collagen orientation in rats: Results from acoustic velocity measurements. J Bone Miner Res 1996;11:1292-301.
12. Hans D, Arlot ME, Schott AM, Roux JP, Kotzki PO, Meunier PJ. DO ultrasound measurements on the os calcis reflect more the bone microarchitecture than the bone mass: A two dimensional histomorphometric study. Bone 1995; 16:295-300.
13. Hans D, Srivastav SK, Singal C, Barkmann R, Njeh CF, Kantorovich E, et al. Does combining the results from multiple bone sites measured by a new quantitative ultrasound device improve discrimination of hip fracture? J Bone Miner Res 1999; 14:644-51.
14. Weiss M,Ben-Shlomo A, Hagag P, Ish-Shalom S. Discrimination of proximal hip fracture by quantitative ultrasound measurement at the radius. Osteoporosis Int 2000;11: 411-6.
15. Hartman C, Shamir R, Eshach-Adiv O, Iosilevsky G, Riva B. Assessment of osteoporosis by quantitative ultrasound versus dual energy x-ray absorptiometry in children with chronic rheumatic diseases. The Journal of Rheumatol 2004;31:981-5.
16. Benitez CL, Schneider DL, Barret-Conner E, Sartoris DJ. Hand ultrasound for osteoporosis screening in postmenopausal women. Osteoporosis Int 2000;11: 203-10.
17. Massie A, Reid DM, Porter RW. Screening for osteoporosis: Comparasion between dual energy x-ray absorptiometry and broadband ultrasound attenuation in perimenopausal women. Osteoporosis Int 1993; 3: 107-10.
18. Flecher RH, Fletcher SW, Wagner EH. Clinical epidemiology. The essential. 2nd ed. Baltimore: Williams and Wilkins,1988: 42-75.
19. Mazess RB, Hanson JA, Bonnick SL. Ultrasound measurements of the os calcis. Bone 1992; 13: 280-
20. Van Daele P.L.A.,Burger H, Algra D, Hofman A, Grobbee D.E, Birgenhager JC,et al. Age-associated changes in ultrasound measurements of the calcaneus in men and women: The Rotterdam Study. J Bone Miner Res1994; 9: 1751-7.
21. Grampp S, Henk C, Lu Y, Krestan C, Resch H, Kainberger F, et al. Quantitative US of the calcaneus: cutoff levels for the distinction of healthy and osteoporotic individuals. Radiology 2001;220: 400-5.

EXTRALUMINAL MIGRATORY UPPER CERVICAL ESOPHAGEAL FISHBONE

Lojana TUNTIYATORN, MD[1]
Chalermchai CHINTRAKARN, MD[2]

ABSTRACT

Ingested foreign bodies which migrate extraluminally are rare occurrences. If untreated, they may result in life threatening complications. The patient presented with a history of swallowing a fishbone which migrated extraluminally. CT is invaluable tool in localizing the foreign body and inflammatory changes of the neighbouring soft tissue for external exploration. We also reviewed sensitivity and specificity of plain radiograph and computed tomography for impacted fishbone.

INTRODUCTION

Fish bones are the most common upper aerodigastric and esophageal foreign body found in adult. Usually these bones can pass through the GI tract, but lodgement can occur at the various areas. Potential complications including esophageal perforation, mediastinitis, cervical or mediastinal abcess, emphysema, esophago-tracheal fistula and sepsis are rare but catastrophic. Extraluminal migration to the parapharyngeal or prevertebral soft tissue requiring an external approach for removal is unusual. Suitable imaging modalities can assist the surgeon in this awkward problem for localization of the site of the migrated fish bone. We present a case of accidental ingestion of the fish bone with penetrating the cervical esophagus and complete extraluminal migration.

CASE REPORT

A 61-year-old women was presented with 1-day history of sudden onset of throat pain after eating fish head. She felt a sensation of foreign body impaction. Although she initially ate large rice bolus in attempt to dislodge a possible retained fish bone, the pain was gradually increased and was associated with odynophagia and dysphonia. She had no cough, fever or respiratory difficulties.

On physical examination, the patient was afebrile and hemodynamically stable. No tenderness, neck mass, cellulitis or lymphadenopathy at the neck can be demonstrated. The oropharynx shows mild enlargement of the tonsils.

Indirect laryngoscope did not found the fishbone or any pathology at the oropharynx, hypopharynx or larynx. The true vocal cord showed normal movement.

Lateral and AP neck radiograph, soft tissue technique were taken. These revealed a thin linear opaque foreign body in the prevertebral space at the level of seventh cervical vertebra associated with soft tissue widening. (Fig.1)

The patient was admitted for exammination under anesthesia. The direct laryngoscope and esophagoscope were performed. The pharynx, larynx and pyriform sinus are unremarkable. There was mild

[1] Department of radiology, Ramathibodi hospital, Mahidol University, Bangkok 10400
[2] Department of otolaryngology, Ramathibodi hospital, Mahidol University, Bangkok 10400

swelling at the posterior wall of the esophagus but no foreign body could be found. Repeated lateral and AP neck, soft tissue technique revealed retained and unchanged in position of the opaque foreign body as well as prevertebral soft tissue swelling. Second direct laryngoscope and esophagoscope were done in the next following day. Still seen was mild inflammation of the posterior wall of the esophagus but no foreign body could be found. Accidentally, minimal mucosal tear at the posterior esophageal wall was done during passing esophagoscope. The procedure was stopped. She developed febrile and tenderness at the thyroid region in the next two following days. Intravenous rehydration and antibiotics were obtained. In order to have a better localization of the foreign body, thin slice contrast axial MDCT scan was performed with coronal and sagittal recontruction. It revealed penetrating fish bone, 15 mm in length at the left prevertebral space adjacent to the posterior wall of the esophagus but external to the esophagus and outside the lumen at C7 level. Associated surrounding thin fluid collection was seen without demonstrable gas or abscess. (Fig.2) The patient was obtained external neck exploration under anesthesia. The fish bone, 1.5 cm in length was found within the left prevertebral soft tissue nearby the carotid artery. The thyroid gland, the left carotid artery and the left recurrent laryngeal nerve are preserved. The fish bone was removed. Recovery was uneventful. Fever, pain and odynophagia were disappeared. The patient was discharged with oral antibiotics.

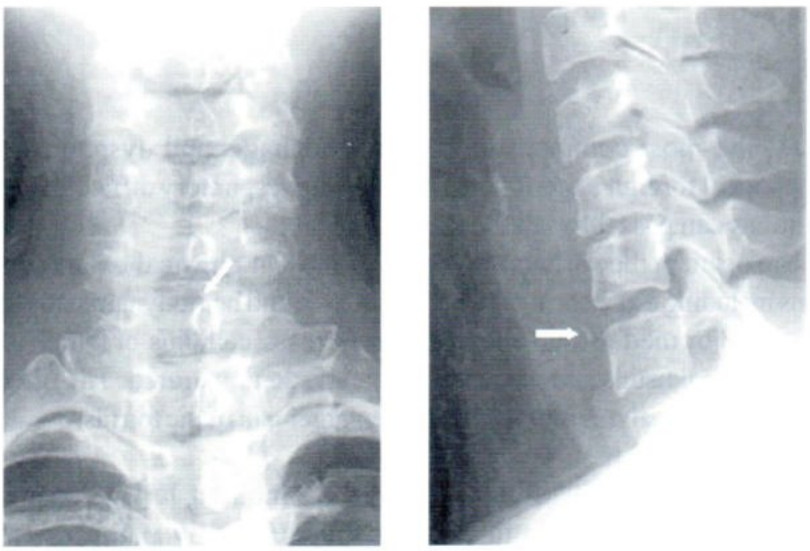

Fig.1 AP and lateral neck soft tissue technique demonstrating radio -opaque fish bone at the prevertebral soft tissue at the level of C7

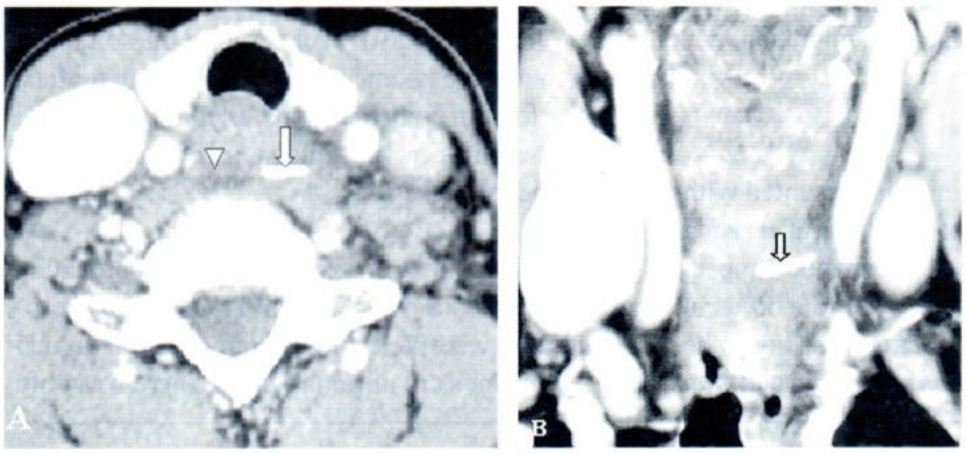

Fig.2 Axial **(A)** and coronal **(B)** computed tomography scan. The fish bone (arrow) is clearly seen outside the esophagus in the left prevertebral space associated with soft tissue edema.(arrowhead)

DISCUSSION (AND REVIEW ARTICLES)

Fish bones are the most common foreign bodies found in upper aerodigastric tracts in adult, comprising 31% of cases found to have retained foreign body. Symptoms including a sudden onset of discomfort while eating, with progressiveness of symptoms, otalgia and unable to swallow saliva are commonly found. The common sites of impaction are tonsils, esophagus, hypopharynx, posterior third of the tongue and vallecula in order of freguencies.[1] Physical examination will catch the majority of the fish bones in tonsils and posterior tongue. It needs emergency fiberoptic laryngoscope or flexible esophagoscope for diagnosis and retrieval in the rest.[2] However it requires a general anesthesia and there is some risk of perforation. To prevent the unnecessary interventions, imagings are commonly ordered to locate the foreign body.

In clinical practice, lateral neck radiography is recommended if mirror examination is difficult or fail to reveal a foreign body. However, Evan RM et al assessed that the sensitivity, specificity and positive value of radiography for impacted fish bone are 25.3%, 86% and 72.7% respectively.[3] Visualization is dependent on the degree of radio-opacity of various species of the bones, size of the bones, location of impaction, orientation of the bone, presence of air and soft tissue swelling around the suspected foreign body. Sea fish bones contain more calcium than fresh water fish bones. The larger fish obviously will have bigger bones. Location in the pyriform sinus and orientation of the bone parallel to the film diminish the visibility.[4,5,6,7] Barium swallowing with cotton pledgets is another imaging in case of negative plain radiography. The major problem is that it coats the esophagus and makes the subseguent esophagoscope or other examination very difficult.

The usefulness of computed tomography in the diagnosis of fishbone impaction in esophagus, presented in Japan (Oct 1997) clearly demonstrated impacted fishbones in all patients but plain X-ray failed to demonstrated in 56% of cases. CT can not only show existence and location of the fishbone but also visualization of the damage or secondarily induced inflammatory changes in the neighbouring structures, such as retropharyngeal abscess. CT can provide very useful information for the diagnosis of dreadful complications, such as mediastinitis, lung abscess, esophageal carotid artery fistula or esophageal aorta fistula.[8] Unenhanced CT with soft tissue and bone windows may replace the barium swallowing because of better detection of thin, small, minimally calcified foreign bodies. In addition, it is readily available, rapid and exposes the patient to less radiation than barium swallowing.[9]

Foreign bodies may be classified as intraluminal, impacted, penetrating or complete extraluminal. Extraluminal migration of foreign body is the most unusual. The cricopharyngeal sphincter region of the cervical esophagus is the common site of perforation.[10] Most penetrating foreign body is typically linear, sharp and pointed type which would logically cause less resistance on traveling through the soft tissue. More irregular shaped foreign bodies such as chicken or duck bones are less likely to migrate through the soft tissue. The previously reports revealed accidental ingestion of sharp metallic object and fishbone with complete extraluminal migration respectively.[11,12]

Our case was presented with extraluminal migration of the fishbone through the cricopharyngeal splinctor region of the cervical esophagus into the left prevertebral space associated with soft tissue edema. The mechanisms by which the foreign body appeared to be propelled through the soft tissue could be due to combination of esophageal peristalsis and ingestion of large bolus of food after impaction. After the fishbone was not found by twice direct laryngoscope and esophagoscope, plain radiography confirmed the presence of the retained fish bone. The CT scan of the neck with and without contrast was the investigation of choice to serve as a road map for localizing

the foreign body. Having confirmed that the foreign body is extraluminal, exploration and removal of the foreign body via the external approach was performed to avoid life threatening complication. She became afebrile and was discharged in the next two days.

Based on this case we would suggest that when a patient presents with a suspected ingested sharp foreign body in the neck, a three-stages approach is used. First, a detail history with a thorough examination of upper airway including indirect and transnasal fiber-optic pharyngolaryngoscopy are to be done. If the foreign body can not be demonstrated, lateral and PA neck radiography are indicated. Secondly, reexammination of the pharynx and esophagus under general anesthesia should be undertaken and the object removed if it is accessible. If the foreign body is not seen in the lumen, CT scan should be considered. Thirdly, external approach may be performed using CT as a road map.

REFERENCE

1. Jones NS, Lannigan FJ, Salama NY. Foreign bodies in the throat:a prospective study of 388 cases. Journal of Laryngology and Otology, February 1991;105:104-108.
2. Murty PSN, Vijendra S, Ramarkrishna S, Fahim A. Foreign bodies in the upper aerodigestive tract. SQU Journal for scientific research: medical science 2002; vol: 3, No: 2: 117-120.
3. Evans RM, Ahuja A, Rthys Williams S, Van Hasselt CA. The lateral neck radiograph in suspected impacted fish bone--does it have a role? Clinical Radiolology. Aug 1992; 46(2): 121-3.
4. Hone SW, Fenton J, Clarke E, Hamilton S, McShane D. The radio-opacity of fishbones: cadaveric study. Clinical Otolaryngology 1995;20(3):234-5
5. Ell SR, Sprigg A. The radio-opacity of fishbones--species variation: Clinical Radiology. 1991Aug;44(2):104-7
6. Kumar M, Joseph G, Kumar S, Clayton M. Fish bone as a foreign body. Journal of Laryngology and Otology, July 2003; 117:568-569
7. Lue AJ, Fang WD, Manolidis S. Use of plain radiography and computed tomography to identify fishbone foreign bodies. Otolaryngol Head Neck Surg 2000;123:435-8.
8. Watanabe K, Kikuchi T, KatoriY, Fujiwara H. The usefulness of computed tomography in the diagnosis of impacted fish bones in the oesophagus. Journal of Laryngology and Otology, April 1998; 112:360-364.
9. Braverman I, Giniru JM, Polv O, Saah D. The role of CT imaging in evaluation of cervical esophageal foreign bodies. Journal of Otolaryngology, Aug 1993;22(4):311-314.
10. Singh B, Kantu M, Har-El G, Lucente FE. Complication associated with 327 foreign bodies of the pharynx, larynx and esophagus. Ann.Otol.Rhinol.Laryngol.1997;106:301-303
11. Lowinger D, Makarie L, Cole I, Szasz J. Retrieval of an extraluminal swallowed sharp foreign body. Aust.N.Z.J.Surg.1999;69:399-402.
12. Al-Shukry SM, A swallowed fishbone penetrating the esophagus into the sternocleidomastoid muscle. SQU Journal for scientific research: medical science 2003; vol 5, no.1 -2: 51-52.

CORONARY ANOMALIES: CASE REPORTS AND LITERATURE REVIEW

Jaturat KANPITTAYA[1] MD, Christoph R BECKER[2] MD, Bernd J WINTERSPERGER[2] MD, Maximilian F REISER[2] MD

ABSTRACT

This was a retrospective, descriptive review and analysis of two cases of coronary anomalies to demonstrate the effectiveness of visualizing coronary anomalies using multislices, computed tomography (MSCT). Unique were: 1) An anomaly of the left circumflex coronary artery arising from the right anterior coronary sinus with an anomalous retro-aortic course. 2) The absence of the common left main coronary arterial trunk, with a split origin at the left anterior descending artery and the left circumflex coronary artery. The ramifications of this report is that coronary anomalies are well depicted using CT, helping to avoid iatrogenic events during coronary interventions.

Keywords: Coronary anomalies; Multislices spiral CT (MSCT); Coronary angiography

INTRODUCTION

The incidence of coronary anomalies in patients undergoing coronary angiography varies between 0.4 and 1.3%.[1-7] Many of these anomalies are clinically benign; however, others are associated with serious morbidity and may cause sudden death.[8] Previous reports indicate that coronary anomalies are involved in 12% of sports-related sudden cardiac deaths vs. 1.2% of non-sports-related deaths.[9-10] We report two coronary anomalies discovered by MSCT coronary angiography.

MATERIAL AND METHOD

Retrospective, descriptive reviews were performed on two cases of coronary anomalies examined by MSCT coronary angiography (using a Somatom 16 scanner) with a 420 ms gantry rotation. The studies were accomplished using retrospective ECG gating. A β-blocker was used to prepare the patients as the target heart rate was ≤ 60 beats per minute. The scan protocol included a 0.75 mm collimation, 120 kV, 750 mAs, with 0.42 s rotations at an 8 s delay, a 1 mm slice thickness, a 0.5 mm distance and a B20f kernel.

The examination area covered the tracheal bifurcation down to the base of the heart while we conducted the preliminary coronary calcium score examination. An additional CT angiography (CTA) study was done with an intravenous contrast injection (110 mL) by which a 4 mL/s flow rate was determined. Image post-processing was done with a maximum intensity projection (MIP) and the reconstructed images included three different planes; similar to standard cardiac catheter projections (viz. the right anterior oblique RAO, the left anterior oblique LAO and the spider view). Additional surface-shaded display images (i.e. in space) were done to obtain more information on the coronary vessels.

[1] Department of Radiology, Srinagarind Hospital, Khon Kaen University, Khon Kaen, 40002, Thailand,
[2] Department of Clinical Radiology, University of Munich-Grosshadern, Munich, 81377, Germany.
Correspondence: Dr. Jaturat Kanpittaya, Department of Radiology, Faculty of Medicine, Khon Kaen University, 40002,THAILAND.

CASE REPORTS

We report on two German nationals in whom anomalies of their coronary vessels were discovered.

The first case was a 65-year-old male with an anomaly of the left circumflex coronary artery (LCX) arising from the right anterior coronary sinus with an anomalous retroaortic course (Figures 1-6). Spotty calcification of the LCX was evident.

The second case was of a 46-year-old male with a missing left main coronary arterial trunk, replaced by a split origin for both the left anterior descending artery (LAD) and LCX (Figures 7-9). Additional findings of spotty calcification of the LAD and long type calcification of the diagonal branch were observed (Figure 8)

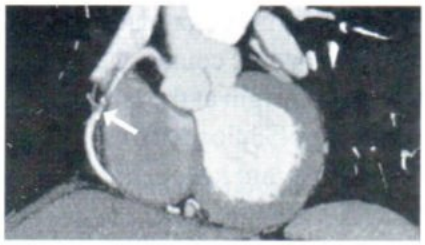

Fig.1 Curved multiplanar reformation (MPR) image of the normal right coronary artery (RCA)

Fig.2 Curved MPR image shows the LCX arising from right coronary sinus

Fig.3 Curved MPR image shows retroaortic course of the LCX

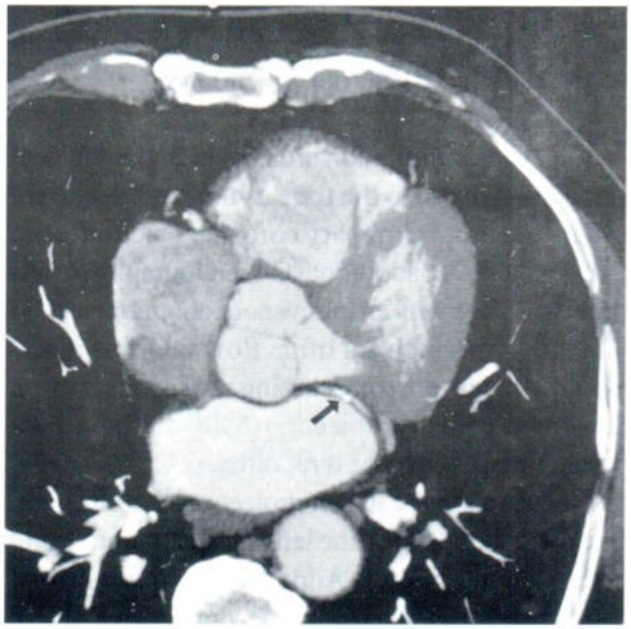

Fig.4 Axial MSCT image displays retro-aortic course of the LCX

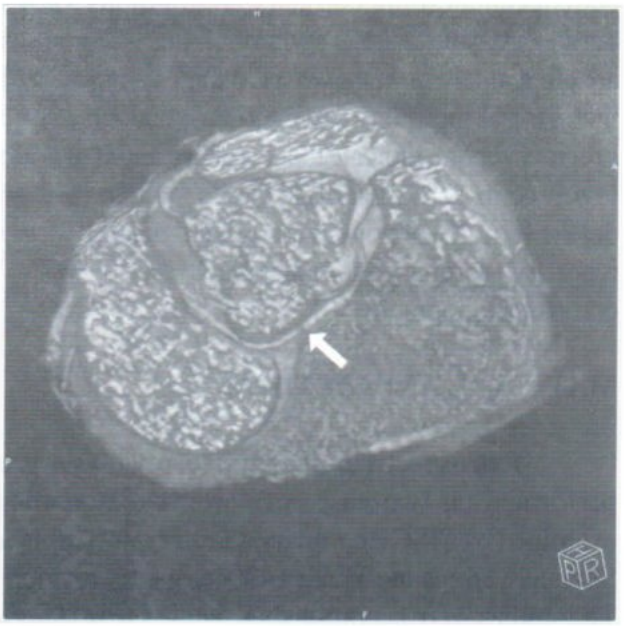

Fig.5 Shaded-surface 3D display of the heart and coronary artery depicts anomaly of the LCX arising from the right coronary sinus with retroaortic course

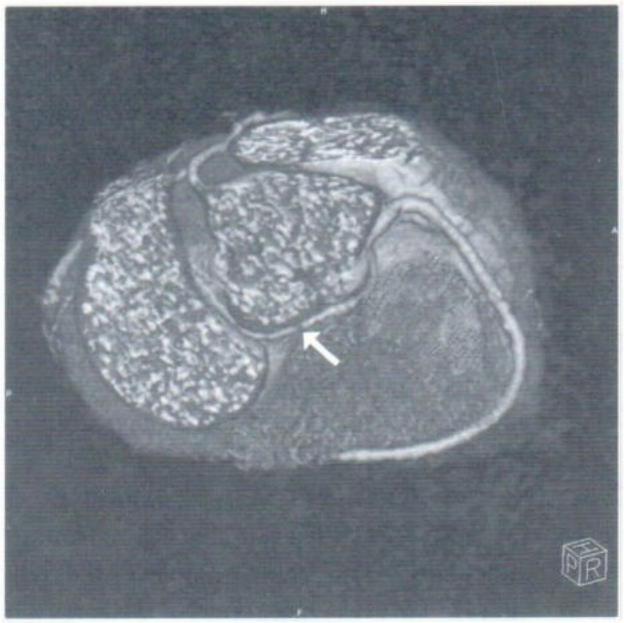

Fig.6 Shaded-surface display image shows retro-aortic course of the LCX

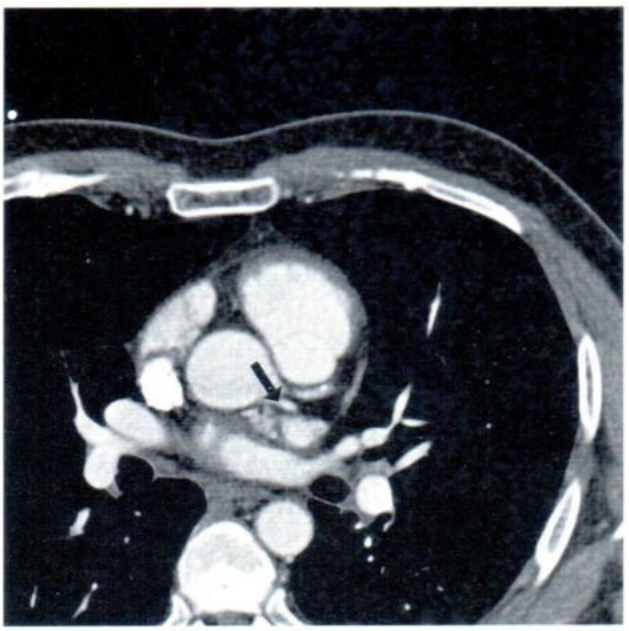

Fig.7 Axial MSCT image shows absent of left main coronary artery and split origin of the LAD and LCX

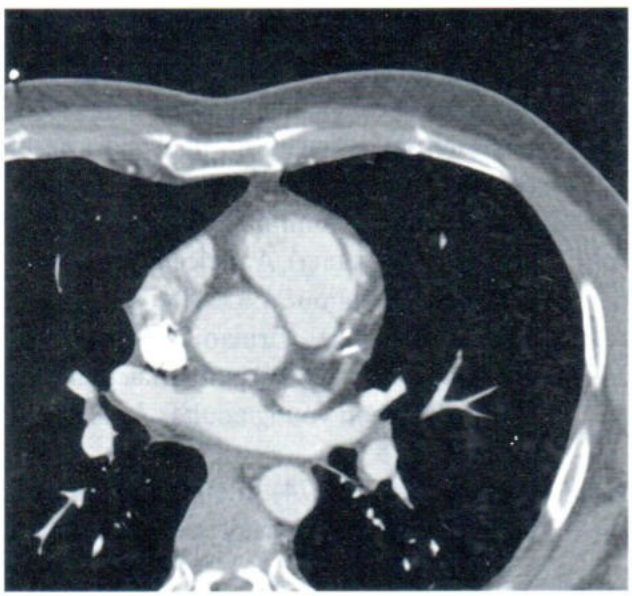

Fig.8 Axial MSCT image displays spotty calcification of the LAD and long type calcification of diagonal branch

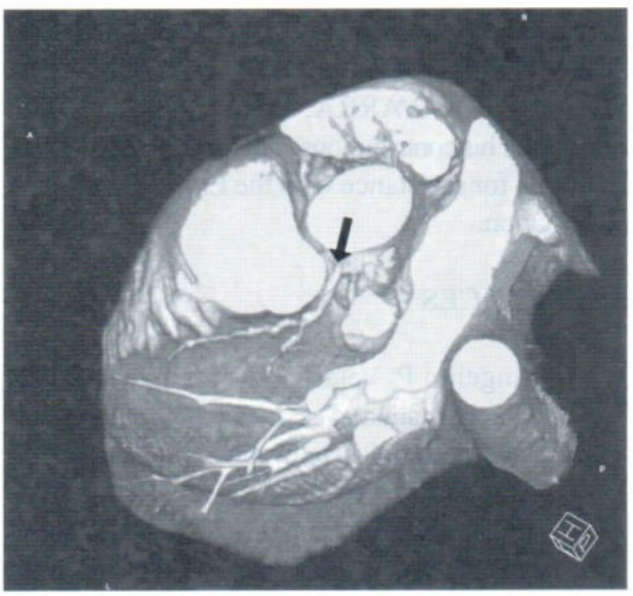

Fig.9 Shaded-surface 3D image demonstrates split origin of the LAD and LCX

DISCUSSION

In adults, congenital coronary anomalies are observed with a frequency of ~0.8%. Among these, the left circumflex coronary artery, originating from the right coronary sinus, comprises of more than half of the anomalies.[11] Some reports indicate a similar split-origin of the LAD and LCX constitutes about 35% of anomalies.[6]

Most patients with coronary anomalies are asymptomatic; however, some are associated with serious morbidity. Knowledgeable awareness of these variations is crucial during invasive catheterization or bypass surgery.

Coronary anomalies are well depicted by MSCT coronary angiography, so the modality is useful for avoiding iatrogenic events during coronary interventions.

ACKNOWLEDGMENTS

The authors thank Gorka BASTARRIKA, DEPARTMENT OF RADIOLOGY, UNIVERSIDAD DE NAVARRA, PAMPLONA, 31008, SPAIN, for his contributions, and Mr. Bryan Roderick Hamman for assistance with the English-language presentation.

REFERENCES

1. Angelini P, Velasco JA, Flamm S (2002) Coronary anomalies. Incidence, pathophysiology, and clinical relevance. Circulation 105: 2449-2454
2. Balfaxe HA, Wixson, D (1977) The incidence of congenital anomalies of the coronary arteries in the adult population. Radiology 122:47-52
3. Yamanaka O, Hobbs RE (1990) Coronary anomalies in 126, 595 patients undergoing coronary angiography. Cathet Cardiovasc Diagn 21:28-40
4. Cieslinski G, Rapprich B, Kober G (1993) Coronary anomalies: incidence and importance. Clin Cardiol 16:711-715
5. Ho JS, Strickman NE (2002) Anomalous origin of the right coronary artery from the left coronary sinus, case report and literature review. Tex Heart Inst J 29:37-39
6. Harikrishnan S, Jacob SP, Tharakan J et al. (2002) Congenital coronary anomalies of origin and distribution in adults: a coronary arteriographic study. Indian Heart J 54:271-275
7. Sosnowski C, Purzycki Z, Antoniak T, Rewicki M (1997) Isolated left coronary artery anomaly: ectopic origin from the right sinus of Valsava- case report. Pol Heart J 47: 328
8. Bestetti RB, Costa RS, Zucolotto S, Oliveira JS (1989) Fatal outcome associated with autopsy proven myocardial bridging of the left anterior descending coronary artery. Eur Heart J 10:573-576
9. Maron BJ, Thompson PD, Puffer JC et al. (1996) Cardiovascular preparticipation screening of competitive athletes: a statement for health professionals from the sudden death committee (clinical cardiology) and congenital cardiac defects committee (cardiovascular disease in the young), American Heart Association. Circulation 94:850-856
10. Burke AP, Farb A, Virmani R et al. (1991) Sports-related and non-sports related sudden cardiac death in young adults. Am Heart J 121:568-575
11. Page HL et al. (1974) Anomalous origin of the left circumflex coronary artery. Circulation 50:768-773

EOSINOPHILIC GRANULOMA OF THE COLON SIMULATING CARCINOMA

Nitaya THONGSIBKAO, M.D.[1]

ABSTRACT

Eosinophilic granuloma of the colon was diagnosed in a 66-year-old woman, presented with chronic abdominal pain. Barium enema study showed concentric mass with sinus tract. Left hemicolectomy was performed because of carcinomatous appearance and the histopathology revealed eosinophilic granulomatous infiltration of the colon.

Keywords: Eosinophilic granuloma, colon, barium enema

INTRODUCTION

Eosinophilic granulomatous infiltration of the gastrointestinal tract is uncommon disease, and frequently involves the stomach and the small intestine. The colon is rarely involved. This is a case report of eosinophilic granuloma of the colon. The contrast radiographic examinations and the histopathology were illustrated.

CASE REPORT

A 66-year-old Thai female patient presented with chronic abdominal pain for 1 year. She was diagnosed to have dyspepsia and relief symptoms by medical treatment. In this admission, she complained about severe left upper quadrant pain.

Physical examination showed left upper quadrant tenderness.

The basic laboratories were normal. There was no leukocytosis or peripheral eosinophilia. CEA was within normal limit. CXR and plain abdomen were unremarkable.

Upper GI study and small bowel follow through revealed diverticula at second and third part of duodenum. The remainders were unremarkable. (Figure 1)

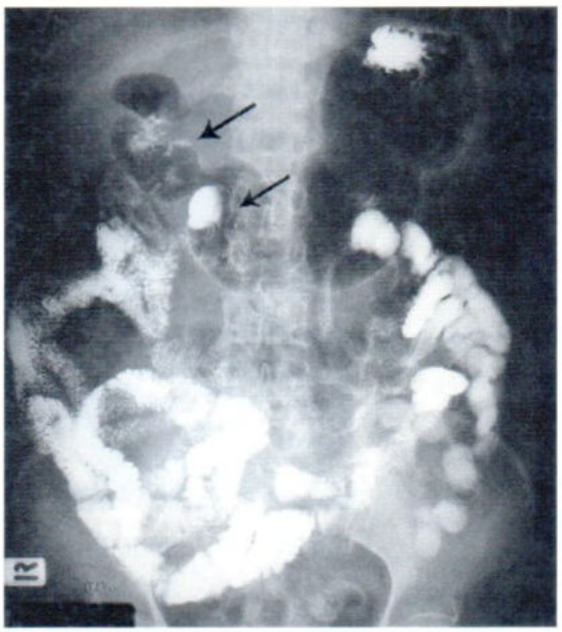

Fig.1 Small bowel follow through shows duodenal diverticula at second and third part (black arrows).

[1] Department of Radiology, Buddhachinnaraj hospital, Muang, Phitsanulok 65000, Thailand.

Barium enema study revealed smooth concentric submucosal mass, 4 cm long, at the descending colon. There was a sinus tract deep to the mass, 1.5 cm long. This radiographic study was mimicking carcinoma. (Figure2-3)

Intraoperatively, 4-cm firm to hard mass of the descending colon was seen. This looked like carcinoma, so that left hemicolectomy was performed.

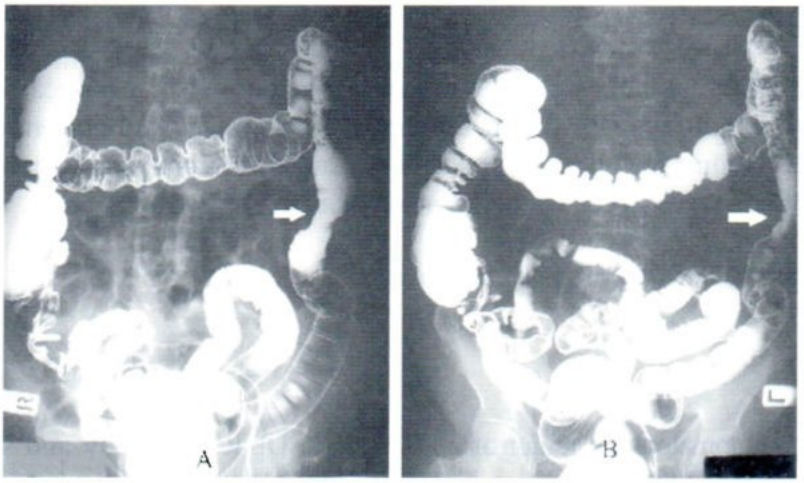

Fig.2 (A and B) Overhead films of barium enema study show concentric submucosal mass at descending colon (white arrows)

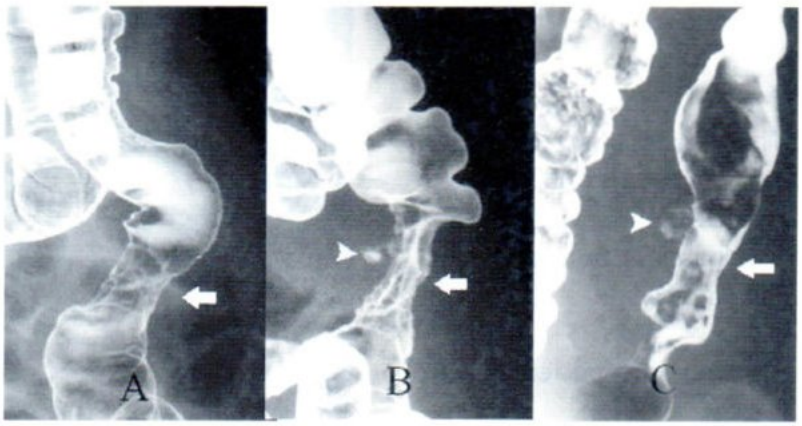

Fig.3 (A-C) Spot films at the lesion of descending colon.

A: Smooth concentric mass (white arrow) represents submucosal lesion.

B: Subsequent film shows sinus tract (arrowhead) deep into the submucosal mass (white arrow)

C: Post-evacuation film shows more barium filled in the sinus tract (arrowhead)

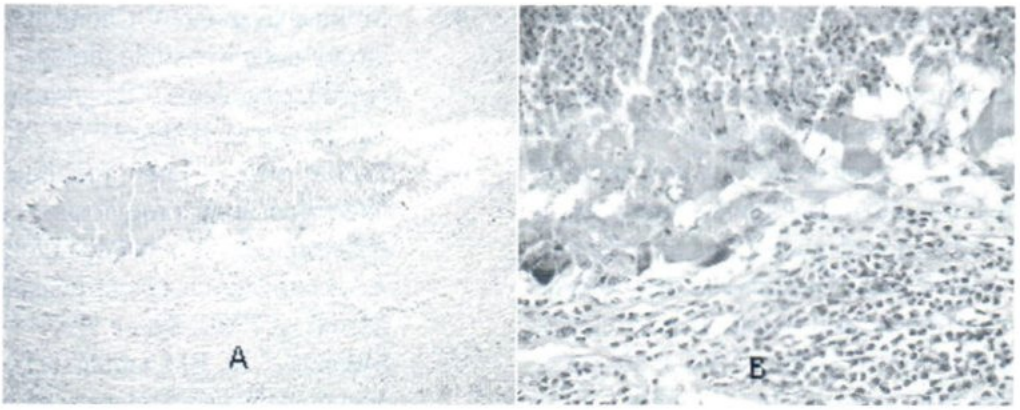

Fig.4A Low magnification demonstrates granuloma with central necrosis.
Fig.4B High magnification reveals granuloma with central neutrophilic aggregates and necrosis. The surrounding tissue exhibits some eosinophils, lymphocytes and plasma cells.

At histopathology, the segment of colon, 34 cm long, showed a 4 cm long infiltrative gray-brown lesion, involving the whole circumference, at 14 cm far from one end. The lesion was 1-2 cm thick and extended to pericolic fat. The lumen was markedly narrow. Some small pericolic lymph nodes, 0.1-0.5 cm in diameter, were dissected. Microscopic examination revealed extensive inflammatory cell infiltration in the bowel wall, including predominantly eosinophils, lymphocytes and plasma cells, as well as some granulomas with central neutrophilic aggregation and necrosis (figures 4). The lesion was most likely parasitic tract, although no parasite was found.

The patient had a complete recovery, postoperatively without complication.

DISCUSSION

Eosinophillic gastroenteritis is an unusual condition, characterized by eosinophillic infiltration of the gastrointestinal tract. The most common sites of involvement are the stomach and the small intestine. The colon and esophagus are rarely involved. About half of patients have allergic disease and there are leukocytosis and peripheral eosinophilia.[22,24-25] Some are associated with causative agents such as parasitic infestations from anisariasis, angiostrongiliasis, gnathostomiasis, hookworm and other nematodes, particularly in the edemic area.[1-2,4-5,14,20-21] This disorder may be associated with autoimmune connective-tissue diseases, such as scleroderma, dermatomyositis and polymyositis.[6,23]

Clinical symptoms are related to the site and extent of the gastrointestinal involvement, such as abdominal pain, nausea, vomiting, GI bleeding, diarrhea, malabsorption, bowel obstruction, bowel perforation and peritonitis.[4,9-13,15-17,19-22]

For this case, eosinophilic granulomatous infiltration of the colon is thought to be caused by parasitic infestation although the larvae or parasites can not be demonstrated at the histopathologic pictures. In the literature, some cases could be diagnosed from a history of raw food or causative fish ingestion for few hours to few days, before the onset of symptom, together with radiologic findings and particularly histopathologic pictures. The remainder could be diagnosed from history, radiologic examination and IgE antibody to the parasite.[1-2,8-9,11,14] Unfortunately, in my institute there is no facilities for serologic examination.

The radiologic findings of eosinophilic gastroenteritis are mucosal edema, nodularities, thickening folds, submucosal mass, narrowing, rigidity and sometimes together with bowel obstruction.[1-2,5,12,14,18] The rarity of eosinophic gastroenteritis, non-specific presenting features and radiologic findings make it easy to be misdiagnosed initially as a malignant tumor,[3,7,19,21] as in this case. The presence of peripheral eosinophilia may be helpful in establishing the diagnosis, but it could be normal in about 25% of the cases. The other disorders that may be accompanied by eosinophilia are for examples parasitic infection, vasculitis, lymphoma, carcinoma or inflammatory bowel diseases. The IgE antibody to parasite is helpful in the suspicious cases.

In conclusion, eosinophic granuloma is one of the differential diagnosis of submucosal mass, among stromal tumors, lymphoma and carcinoma particularly in the patient, who resides in the endemic area of parasitic infestation or who has allergic history.

ACKNOWLEDGEMENT

The author would like to thank Assistant professor Wittanee Na Chiangmai, Faculty of Medicine, Chiangmai University, for her comment and Dr.Suchat Porncharoenpong, Department of pathology, Buddhachinnaraj Hospital, for the histopathology.

REFERENCE

1. Matsumoto T, Iida M, Kimura Y,Tanaka K, Kitada T, Fujishima M. Anisakiasis of the colon: radiologic and endoscopic features in six patients : Radiology 1992; 183(1): 97-99
2. Matsui T, Iida M, Murakami M, Kimura Y, Fujishima M,Yao Y,Tsuji M. Intestinal anisakiasis: clinical and radiologic features. Radiology 1985; 157(2) 299-302
3. Zimmerman HG. Eosinophilic granuloma of the ascending colon. Z Gastroenterol.1977; 15(11): 676-9
4. Sirikulchayanonta V, Chongchitnant N. Gnathostomiasis: a possible etiologic agent of eosinophilic granuloma of the gastrointestinal tract. Am J Trop Med Hyg 1979; 28(1): 42-4
5. Loria-Cortes R, Lobo-Sanahuja JF. Clinical abdominal angiostrogylosis. A study of 116 children with intestinal granuloma caused by Angiostrongylus costaricensis. Am J Trop Med Hyg 1980; 29(4): 538-44
6. Memain N, De BM, Guillevin L, Wechsler B, Meyer O. Delayed relapse of Churg-Strauss syndrome manifesting as colon ulcers with mucosal granuloma: 3 cases. J Rheumatol 2002; 29 (2): 388-91
7. Yoh H, Natsugoe S,OhsakoT, Yamada K et al. Eosinophilic granuloma of the stomach mimicking gastric cancer, report of a case. Hepatogastroenterology. 2001; 48 (38): 606-8
8. Pampiglione S, Rivasi F, Criscuolo M, De Benedittis A, et al. Human anisakiasus in Italy: a report of eleven new cases. Pathol Res pract. 2002; 198(6): 429-34
9. Couture C, measures L,Gagnon J, Desbiens C. Human intestinal anisakiosis due to consumption of raw salmon. Am J surg Pathol 2003; 27 (8): 1167-72
10. Caramello P, Vitali A, Canta F, Caldana A, Santi F,Caputo A, Lipani F, Balbiano R. Intestinal localization of anisakiasis manifested as acute abdomen. Clin Microbiol infect 2003; 9(7): 734-7
11. Schuster R, Petrini JL, Choi R. Anisakiasis of the colon presenting as bowel obstruction. Am Surg 2003; 69 (4): 350-2
12. Waisberg J, Corsi CE, Rebelo MV, Bromberg SH, et al. Jejunal perforation caused by abdominal angiostrongyliasis. Rev Inst Med Trop Sao Paulo 1999; 41(5): 325-8
13. Silvera CT, Ghali VS, Roven S, Heimann J, Gelb A. Angiostrongyliasis : a rare cause of gastrointestinal hemorrhage. Am J Gastroenterol 1989; 84(3): 329-32

14. Bouree P, Paugam A, Petithory JC. Anisakidosis: report of 25 cases and review of the literature. Comp Immunol Microbiol Infect Dis 1995; 18 (2): 75-84
15. Hemsrichart V. Intestinal anisakiasis: first reported case in Thailand. J Med Assoc Thai 1993; 76(2): 117-21
16. Sasaki T, Fukumori D, Matsumoto H, Ohmori H, Yamamoto F. Small bowel obstruction caused by anisakiasis of the small intestine: report of a case. Surg Today 2003; 33(2): 123-5
17. Yoh H, Natsugoe S, Ohsako T, Suenaga T, Hokita S, et al. Eosinophilic granuloma of the stomach mimicking gastric cancer, report of a case. Hepatogastroenterology. 2001; 48 (38): 606-8
18. Judy A, James H. Anisakiasis. Clinical Microbiology Reviews 1989; 2: 278-284
19. Shirahara M, Koga T, Uchida S. Colonic anisakiasis simulating carcinoma of the colon. AJR 1990; 155: 895
20. Ratanarapee S, Jesadapatarakul S. A case of gnathostomiasis simulating acute appendicitis. J Med Assoc Thai 1982; 65 (8): 443-7
21. Laohapand T, Sonakul D, Lolekha S, Dharamadach A. Gnathostomiasis of the colon simulating malignancy: a case report. J Med Assoc Thai 1981; 64(4): 192-5
22. Cello JP. Eosinophilic gastroenteritis: a complex disease entity. Am J Med 1979; 67: 1097-1104
23. Waxman I, Compton CC. Case Records of the Massachusetts general Hospital. The new England Journal of medicine 1993; 329: 343-349
24. Edelman MJ, March JL. Eosinophillic gastroenteritis. AJR 1964; 9: 773-778
25. Goldberg HI, O'Kieffe D, Jenis EH, et al. Diffuse eosinophilic gastroenteritis. AJR 1973; 119: 342-351